

REPLY TO REVIEWER #1:

We thank the reviewer for the comments that helped us to improve the manuscript.

1. The logic (the same as applied in Seifert et al. 2010) is to derive the autoconversion and accretion enhancements for the 2-moment scheme of Seifert and Beheng, and then to use the modified 2-moment scheme in LES simulations. I feel this is a justifiable methodology (especially considering the expense of the bin scheme), but I feel the 1D kinematic model of Seifert and Stevens might not be sufficient to validate the 2-moment implementation. To me, the key difference between bin and 2-moment scheme is the representation of droplet sedimentation (mass/number weighted in the 2-moment scheme and different for every bin in the bin scheme). Thus, the surface rainfall (e.g., Fig. 4 in the current manuscript) may agree well in the 1D test, but may differ more significantly in a test where horizontal variability is included, for instance, in a 2D kinematic test. Overall, I feel the difference in the sedimentation between bulk and bin schemes deserves a closer look, not necessary in the context of the current paper, but in a more general study. I would like to see this aspect at least to be recognized in the current draft.

We agree with the reviewer that a 2D framework would be a much better test and fully agree with the statement concerning sedimentation. We have added a sentence at the beginning of section 4 reading

Although the 1D model provides a reasonable idealized framework for such a test, we would recommend to use a kinematic 2D model (e.g. Szumowski et al. 1998, Morrison and Grabowski 2007) in future studies, because the 1d framework might not be sensitive enough to differences in the treatment of sedimentation which are more relevant in a more complex flow field. Here we apply the simpler 1D model for consistency with Seifert et al. (2010).

2. The fact that differences in the cloud microphysics (i.e., rain formation in the current study) may affect cloud dynamics is obvious. However, this aspect is not even mentioned in the current

manuscript except for (relatively obscure and not discussed) references to the inversion height shown in Fig. 6. I think some discussion of the feedback from the microphysics to the cloud field dynamics (e.g., deepening of the cloud field that is an unfortunate feature of the RICO setup) should be added to the manuscript. Overall, separation of purely microphysical effects from the impact on cloud dynamics is difficult, but needs to be done to fully understand the impacts. Again, I feel just mentioning this issue and leaving it for a future study (perhaps applying the piggybacking method that Grabowski used in his studies published in JAS in 2014 and 2015) would be sufficient. A hint of the dynamic feedback can perhaps be shown by adding the inversion height to time evolutions shown in Fig. 5.

The deepening of the cloud layer is one of the most interesting features of the RICO case and makes it especially valuable when investigating the effects of cloud microphysics on the evolution of the cloud layer. The effect of different microphysical choices or assumptions on the boundary layer dynamics has been extensively discussed by Stevens and Seifert (2008), van Zanten et al. (2011), Seifert et al. (2015) and others. Therefore we have not discussed this in detail in the current manuscript. In the revised version we follow the recommendation of the reviewer and have added the inversion height to Fig. 5 and included a few sentences in section 5.2. reading

The main feedback of the different microphysical developments on the dynamics and evolution of the boundary layer as a whole is that rain formation arrests the growth of the cloud layer as it can be seen in the time series of the inversion height in Fig. 5, i.e., the Ayala-Wang kernel leads to a much shallow cloud layer in the precipitating regime. A similar behavior for different cloud droplet number densities was shown by Stevens and Seifert (2008). For the RICO case the boundary layer deepens and supports successively deeper clouds until moisture is efficiently removed by precipitation. Eventually the precipitating regime reaches a quasi-stationary state, the subsiding radiative-convective equilibrium (Seifert et al., 2015).

Using the piggybacking methodology would be an attractive alternative to our extensive LES study. Without piggybacking the randomness of the individual LES runs makes it actually necessary to use ensembles of LES realisa-

tions, which is computationally very demanding. We agree with the reviewer that piggybacking offers an attractive method to overcome such problems. Nevertheless, we refrained from using the method because it leads to inconsistencies between the dynamics and the microphysics and the results have to be interpreted very carefully. The old fashioned brute force approach used in our study is maybe less elegant, but each simulation is physically fully consistent. Nevertheless, we fully agree that such studies as presented in our manuscript could benefit from the piggybacking approach, if it is carefully used and interpreted.

3. P. 3, paragraph starting at l. 30. The way enhancements are shown in Fig. 1 does not allow seeing the enhancement for droplets of equal (or very close) size. Can you show the enhancement for equal-size droplets for the two formulations? How important are such collisions for the acceleration of rain formation?

The enhancement factor for equal-size droplets is by definition infinite. We would refer to Fig. 4 and section 4.3 of the accompanying paper by Onishi and Seifert (2016, ACP) for a discussion of the collision frequency of similar sized droplets. We think that such collisions, e.g. selfcollection events of small raindrops, are very important especially in maritime clouds with low to moderate cloud droplet numbers and relatively high autoconversion rate. In such clouds small drizzle drops can be present in abundance, but their growth is relatively slow due to the low to moderate cloud water content (limiting accretion) and the rare collisions between similar sized drops (limiting selfcollection). As soon as some drops grow due to some selfcollection events, they also have an advantage in accretion due to the larger fall speed of a bigger drop. Such a chain of processes is what we postulate to explain the increase in accretion rate (Eq. 15), which is stronger than the enhancement of the kernel itself for the accretion process. Or in other words: The enhancement of the collision rate of similar-sized drops leads to a modification of the drop size distribution (a stronger tail) due to selfcollection which is part of the enhancement of accretion parameterized by Eq. (15).

The importance of selfcollection for the surface rain rate in maritime shallow cumulus is also discussed in the recent paper by Naumann et al. (2016) by applying a detailed diagnostics using a Lagrangian drop model (aka superdroplets).

4. P. 4, the end of section 4. I think you can explicitly say when discussing Fig. 4 that the differences are about 10-20 % max, a relatively small difference considering differences seen in cloud field simulations.

Figure 4 is not only there to show that the bulk scheme works reasonably well, but also and maybe more important to discuss the differences between the two collection kernels. It is not clear to which of the two the reviewer refers. The difference between the Ayala-Wang kernel and the Onishi kernel can actually be a factor of 2 (for moderate dissipation rates).

5. P. 7, discussion around l. 29. I think the discussion has to do with the undesirable aspect of the RICO case, namely, the deepening of the cloud field. Perhaps this should be openly stated (I think it is not obvious to someone not familiar with the RICO case). My suggestion at the end of 2 above would also help to make this obvious.

Following the recommendation of the reviewer, we have included a discussion of the deepening of the cloud layer in section 5.2. Nevertheless, we do not understand why the deepening of the cloud field should be 'undesirable'. As long as the subsidence drying is not able to compensate the moisture input from the latent heat flux the cloud layer has to grow. We could agree with the statement that the growth of the cloud layer is artificially slow in the RICO case making it much more susceptible to microphysical perturbations than a boundary layer in which local radiative cooling leads to a more rapid equilibration of the cloud layer, i.e., the deepening should be much more efficient than in the standard RICO case used here.

6. P. 8, text between l. 10 and 15. I feel more explanation is needed here. What is σ_x (mean standard deviation from the time average?). What is the lag-1 auto-correlation? How many samples are there in the 6-hour time series? This method of assessing statistical significance is different from the Student t-test statistic, correct?

Yes, the domain mean quantities are simple time series and σ_x is the standard deviation as it is explained in the text. The standard deviation of a

time series is always 'the mean standard deviation from the time average'. The lag-1 autocorrelation of a discrete time series is the autocorrelation between subsequent samples of that time series. This is standard terminology in statistics and time series analysis (and easily found in most textbooks). Software packages like R, Matlab, NCL, etc. provide functions to calculate these quantities. The estimation of the effective sample size is a classic problem in statistics and the reference provided in the paper gives a more detailed discussion of this topic.

The number of independent samples depends on the quantity, because different variables have different autocorrelation time scales. For the rain rate the effective sample size in a 6-hour time series is between 3 and 10 with an average of about 6. This makes sense as a shallow convective rain event has a typical duration (or time scale) of 1 hour. For the inversion height the sample size is only 1 per 6-hour time series, because the inversion height is the result of the combined action of all boundary layer eddies (i.e. all clouds), i.e., each LES run provides only 1 independent estimate for the inversion height. Due to this averaging property the standard deviation of the inversion height is also much smaller and consequently the standard error is small although the effective sample size is only 1 per LES run. Knowing the effective sample size is a prerequisite for the Student t-test, but we decided to plot only the standard error and not to delve deeper into test for statistical significance. We would argue that even without doing statistical hypothesis testing our analysis is still more elaborate than what is usually presented when comparing different LES runs.

7. P. 10, l. 30. Here is an example of the microphysics-dynamics feedback that is important in this problem, yet it is really not discussed in the current draft.

This feedback is now mentioned several times in the revised manuscript. For a detailed discussion of the basic behavior we refer to the literature, e.g., Stevens and Seifert (2008) as well as Seifert et al. (2015).

REPLY TO REVIEWER #2:

We thank the reviewer for the comments that helped us to improve the manuscript.

Why enhancement factors for autoconversion and time t_{10} are presented for Onishi kernel only? How they differ for Ayala-Wang kernel? Accumulated surface precipitations in 1D for both kernels agree with the proposed parameterization, but are very different. This additional analysis, supplementing that of Onishi and Seifert (2016) discussed in the present text would be of value.

In the revised version we have included the corresponding plots for the Ayala-Wang kernel and extended the discussion of the enhancement factor for the autoconversion rate.

The different autoconversion enhancement factors for the two kernels and the quality of the fits is shown by Fig. 2 in which also the Reynolds number dependency is shown in more detail. The results for the Ayala-Wang kernel show somewhat higher enhancement factors compared to Seifert et al. (2010), mostly due to the improved treatment of the collision efficiency (cf. Onishi and Seifert 2016). The Onishi kernel shows much lower enhancement factors and the maximum is shifted to larger (mean) droplet radii compared to the Ayala-Wang kernel. The Re_λ -dependency reveals that especially for the Onishi kernel the value of the exponent, $p = -1/8$, is really just a fit with limited physical meaning as the actual slope has significant dependencies on \bar{r}_c and Re_λ . This more complicated behavior is consistent with the analysis presented by Onishi and Seifert (2016) who showed that the Reynolds number dependency of the kernel varies with Stokes number (e.g. their Figure 2). For the Ayala-Wang kernel the numerical data shows a steeper increase with Re_λ compared to the parameterization. This is mostly because we kept the exponent at $p = 1/4$ as in Seifert et al. (2010), although the extended range of the dissipation rate in the current study would ask for a slightly higher exponent. The dependency on dissipation rate is assumed to be linear in Eq. (10) and this is confirmed for the Onishi kernel, but for the Ayala-Wang kernel the ϵ -dependency becomes weaker for high dissipation rates.

Analysis of LES results is insufficient. In particular, the authors

discuss basic micro- physical and cloud field parameters between 24 and 30 hours of simulations (Figs. 6 and 8) without paying sufficient attention to cloud patterns, cloud fields, vertical profiles. In effect information on the effects of proposed parameterization / collection kernels on convection dynamics is partially missing. Figure 5 suggests that for several cases there is a significant variability within the last hours of the simulations, which is confirmed in transition times presented in Fig. 7. Extended discussion of the differences would add to the paper.

The different assumptions for the collection kernel and the resulting modification of the warm rain process do not fundamentally change the behavior of the cloud dynamics, i.e., an enhancement of the warm rain process by taking into account turbulence effects on collisions has a very similar effect on cloud patterns, cloud fields, vertical profiles etc. as a change in the cloud droplet number. The latter experiments have been extensively described and discussed in the literature, e.g., by Stevens and Seifert (2008), van Zanten et al. (2011), Seifert and Heus (2013), Seifert et al. (2015) and others. Therefore we present only those aspects of the simulations which help us to learn something new and gain a deeper understanding of the interaction of turbulence and warm rain processes. An example is the response of the accretion-autoconversion ratio to the different kernel assumptions discussed in section 5.3 and 5.4. Specific aspects of the cloud dynamics for the turbulence effects, like the fact that the highest dissipation rates are observed near cloud top, are already discussed in Seifert et al. (2010) and Wyszogrodzki et al. (2013) and there is no reason to repeat this in the current manuscript. A more detailed analysis of the resolved in-cloud turbulence and its effect on rain formation would be very interesting and, in our opinion, new, but is beyond the scope of the current manuscript.

REPLY TO REVIEWER #3:

We thank the reviewer for the comments that helped us to improve the manuscript.

1. The starting point of the paper is the introduction of two collection kernels. Fig. 1 shows how the Reynolds number affects the change of kernel in each case. For most regions, the Ayala-Wang kernel seems to have a more stronger Reynolds number effect. Is there any region in Fig. 1 f) showing a stronger dependence compared to Fig. 1 c). If so, can the reason be provided?

For the details of the collection kernels we refer to the accompanying paper by Onishi and Seifert (2016, ACP). The Onishi kernel shows a strong Reynolds number dependency for small regions in Fig. 1f, mostly along the diagonal, i.e., for droplets of similar size. This is due to the Reynolds number dependency of the optimal Stokes number for the preferential concentration effect. It is postulated that the optimum value for the preferential concentration shifts from $St = 1$ to slightly higher Stokes numbers for high Taylor-microscale Reynolds numbers. Due to the fact that the flanks of the radial distribution function g_{11} , which quantifies the preferential concentration effect, are quite steep a shift in g_{11} leads to a strong increase (or decrease) in a narrow range of drop sizes (Stokes numbers). This is basically what we see in Figure 1f.

2. The paper relies heavily on the contents in other papers including basic definitions. For example, the precise definitions of auto-conversion, accretion, and selfcollection are not given. It would be useful to provide definitions of such.

Yes, this paper is intended for scientists who are familiar with the basic concepts of cloud physics, bulk microphysical parameterizations and turbulence effects on collision rates. It is hardly possible to review all those topics in a scientific paper. Nevertheless, we provide a short introduction of essential definitions and relations for particle-laden turbulence in section 2. For the basic ideas and definition of warm rain bulk microphysics we would like to refer to Klaus Beheng's review paper

Beheng, K. D.: The evolution of raindrop spectra: A review of basic microphysical essentials, Rainfall: State of the Science, Geophys. Monogr., 191, 2948, 2010.

but following the request of the reviewer we have extended the introduction of the bulk microphysics scheme at the beginning of section 3, which now provides a short introduction to bulk microphysics parameterizations.

3. Furthermore, regarding the enhancement of accretion and self-collision k_{rr} , I assume this factor is used in determining the mean size of rain drops. Can an equation like Eq. (8) be provided to show how k_{rr} is actually incorporated in the moment methods.

In the revised version of the manuscript these equations are explicitly given in section 4. This actually helped to fix some minor inconsistencies in the presentation.

4. One of the observations is that the Ayala-Wang kernel lead to faster autoconversion and Onishis leads to faster accretion. The faster autoconversion is due to stronger Re dependence. Can the reason for faster accretion for the Onishis kernel be provided? This could be discussed in terms of aspects related to the point 1 above.

This is discussed in detail in the accompanying paper by Onishi and Seifert (2016, ACP). As already explained in the answer to question 1, the main effect is the shift of the preferential concentration optimum to higher Stokes numbers in case of high Taylor-microscale Reynolds numbers. The larger Stokes numbers correspond to larger drops which belong to the raindrop category of the bulk scheme.

5. The study uses a single mass (2.6×10^{-10} kg or about $40 \mu\text{m}$ in radius) as the dividing size between cloud droplets and rain drops. I wonder how this choice affects the conclusions of the paper. Can the authors study other dividing size such as $25 \mu\text{m}$ or $35 \mu\text{m}$ as the dividing size? This is important since a very rough moment method is used in the LES.

The threshold size is not arbitrarily chosen, but corresponds to the mini-

imum of the bi-modal mass distribution function during the evolution of the drop size distribution (see e.g. Fig. 4 of Beheng’s review paper). A small change like using 35 μm instead of 40 μm will not affect the results as this will only change the autoconversion rate by about 10 %. A reduction to 25 μm is inconsistent with the assumptions made in SB2001 and simply too small for the separating size of a two-category scheme. To explicitly predict the formation of such small drizzle drops the three-category scheme of Sant et al. (2013, J. Atmos. Sci) could be used instead. For shallow cumulus clouds this is not necessary, but it might be interesting for stratocumulus.

6. The formulation involves a shape parameter (Eq. 7). I assume A and B are related to L_c and x_c . It is not clear if ν is kept as a constant during the LES simulation and how ν is determined. Can this be clarified?

Yes, the gamma shape parameter of the cloud droplet distribution ν is constant during an LES simulation. We mention this explicitly in the revised manuscript in section 5.1. The meaning of this constant ν in the SB2001 scheme is often misunderstood as it is actually only the shape parameter before coagulation kicks in. It would be possible to estimate a local time-dependent ν which is consistent with the assumption of the SB2001 model from the universal function $\Phi_{au}(\tau)$ or simply as a function of τ . Here τ is the non-dimensional internal time variable of the system, which describes the evolution of the cloud droplet distribution due to coagulation. The autoconversion rate, Eq. (8), is not simply the solution of the collision integral for a fixed ν , but includes the change in the drop size distribution and, hence, an evolving ν . On the other hand, the cloud droplet distribution is not strictly a gamma distribution during coagulation, and therefore estimating ν would provide only limited information (especially the tail of the distribution is much more important than the shape described by ν).

7. In the model equation (10), a single exponent p is used for the whole range of Re . In reality, the collection kernel (specifically the RDF) first increases with Re , then saturates or decreases slowly with Re . The question is then how valid a single exponent in representing the effect of flow Re .

Given the various approximations and uncertainties in the kernel, the bulk

scheme and the LES model, and the sensitivity to grid resolution of the LES, we would argue that the use of a single exponent p to describe the Re-dependency is a minor problem. For a true reference simulation we would need an LES model that can predict ϵ and Re_λ independently. Having such a model we could then think about using a super-droplet approach to simulate the coagulation explicitly with the full Onishi kernel.

8. Another observation is that the Ayala-Wang kernel leads to shallow inversion height. However, in Wyszogrodzki et al. (2013) and Grabowski et al. (2015, Atmos. Chem. Phys., 15: 913-926) based on the spectral bin method, it is shown the dynamic effect of faster droplet growth is a deep cloud top. I wonder if these two are contradictory, and if the reason for this contradiction is due to their use of the moment method. Clearly, the strong sensitivity of the collision kernel with droplet size and shape of droplet size distribution requires a more accurate representation than the two-moment method. The authors should clarify the various errors associated with the moment method, and potential effect on the conclusions of the paper.

This is maybe related to the simulation of the BOMEX case (by Wyszogrodzki et al. 2013 and Grabowski et al. 2015) vs the RICO case that is used here and has been used in Seifert et al. (2010). In addition the domain used by Wyszogrodzki et al. (2013) is quite small with only 6.4 km in the horizontal compared to 51.2 km in the current study, and the simulated time period is only 6 h in Wyszogrodzki et al. (2013) compared to at least 30 h in the current study. For example, the small domain may be dominated by individual clouds which can lead to a different interpretation of the results. Maybe more important, the BOMEX case was initially set up as a non-precipitating case and the system is in equilibrium without the formation of precipitation (Siebesma et al. 2003, JAS). Hence, the formation rain leads to a perturbation of this quasi-equilibrium state and pushes the system into an instationary transient state. In contrast, RICO is not in equilibrium without rain as it was designed based on data from a rainy period. The RICO case approaches a quasi-equilibrium only due to the formation of rain late in the simulations. These differences in the model setup and the case design can lead to quite different behavior and different interpretations. It would be very interesting to do an intercomparison with both cases us-

ing spectral bin and bulk methods. Unfortunately, it is very expensive and time consuming to do large sensitivity studies with bin microphysics models. Comparing just a few simulations is very questionable due to the strong sensitivity and randomness of precipitating shallow convection, especially in the RICO case.

We have tried our best to convince the reader that the moments method provides a reasonable parameterization of the collision-coalescence process, e.g., with help of Figs. 3 and 4. A full quantification of the errors is beyond the scope of the paper. Nevertheless, we are confident that the results are qualitatively meaningful and provide valuable insights in the behavior of precipitating shallow convection and the turbulence effect on rain formation. As suggested by the the analysis presented in section 5.4 the largest uncertainty of the model might actually be associated with the still too coarse resolution of the LES model.

Turbulence effects on warm rain formation in precipitating shallow convection revisited

Axel Seifert¹ and Ryo Onishi²

¹Deutscher Wetterdienst, Offenbach, Germany

²Center for Earth Information Science and Technology, Japan Agency for Marine-Earth Science and Technology, Yokohama Kanagawa, Japan

Correspondence to: Dr. Axel Seifert (axel.seifert@dwd.de)

Abstract. Two different collection kernels which include turbulence effects on the collision rate of liquid droplets are used as a basis to develop a parameterization of the warm rain processes autoconversion, accretion and selfcollection. The new parameterization is tested and validated with help of a 1D bin microphysics model. Large-eddy simulations of the rain formation in shallow cumulus clouds confirm previous results that turbulence effects can significantly enhance the development of rain water in clouds and the occurrence and amount of surface precipitation. The detailed behavior differs significantly for the two turbulence models revealing a considerable uncertainty in our understanding of such effects. In addition, the large-eddy simulations show a pronounced sensitivity to grid resolution which suggests that besides the effect of sub-grid small scale isotropic turbulence which is parameterized as part of the collection kernel also the larger turbulent eddies play an important role for the formation of rain in shallow clouds.

10 1 Introduction

The formation of rain in warm liquid clouds is a result of the condensational growth on cloud condensation nuclei, and the subsequent growth of these droplets by binary collisions (Beard and Ochs, 1993; Pruppacher and Klett, 1997; Beheng, 2010). Especially in strongly turbulent clouds, like cumulus convection, the in-cloud turbulence can potentially increase the frequency of such binary collisions and thereby enhance rain formation (Devenish et al., 2012; Grabowski and Wang, 2013). This problem has attracted considerable attention over the last two decades culminating in the formulation of the semi-empirical collision-coalescence kernel of Ayala and Wang (Ayala et al., 2008b, a; Wang et al., 2008). This collection kernel attempts to provide a complete and quantitative description of the collision processes in turbulent (warm) clouds. Subsequently, Seifert et al. (2010) have applied this kernel and formulated a two-moment bulk microphysical model that takes into account the turbulence effects on autoconversion and accretion as predicted by the Ayala-Wang kernel. In large-eddy simulations (LES) of trade wind cumulus convection Seifert et al. (2010) have shown a significant impact of the turbulence effect on in-cloud rain formation and surface rain rates. These results, which were based on a two-moment bulk scheme, have later been largely confirmed by Wyszogrodzki et al. (2013) using a bin microphysics model in an LES.

The semi-empirical collision-coalescence kernel of Ayala and Wang is to a large extent based on the results of direct numerical simulation (DNS) which are necessary to quantify the turbulence effects on the collision statistics in terms of, e.g.,

the radial distribution function to describe the preferential concentration effect. As the DNS results are obtained at fairly low Reynolds number, much lower than observed within clouds, the formulation of the collection kernel includes an extrapolation to large Reynolds numbers. An alternative collection kernel recently proposed by Onishi et al. (2015) yields similar results at low Reynolds numbers where DNS data is available, but differs significantly in the Reynolds number dependency and the predicted values at high Reynolds numbers (Onishi and Seifert, 2016).

In the following we revisit the results of Seifert et al. (2010) and repeat most of their study, but now we apply the Onishi kernel and an updated version of the Ayala-Wang kernel. First, we derive and validate the corresponding two-moment bulk schemes, which already allows us some insights into the differences between the two kernels. Next, we apply the two bulk scheme in a large-eddy simulation study to test whether the differences between the two kernels matter in LES of trade wind cumulus clouds.

The structure of this paper very much follows in the steps of the Seifert et al. (2010) study. After a short review of the basic relations the two collection kernels are presented in section 2. In section 3 we use a box model to derive the enhancement factor for autoconversion. In section 4 the two-moment scheme is applied and validated in a 1D kinematic model. The large-eddy simulations are presented and discussed in section 5 followed by the Conclusions.

2 Parameterizations of the turbulence effects in the collision-coalescence kernel

For pure gravitational collisions the collection kernel can be written as (see e.g. Pruppacher and Klett, 1997)

$$K_{\text{grav}}(r_1, r_2) = \pi [r_1 + r_2]^2 |v(r_1) - v(r_2)| E_{\text{coll}} \quad (1)$$

where r_1 and r_2 are the radii of the two droplets, $v(r)$ is the terminal fall velocity of droplets, and E_{coll} is the collision efficiency. For a turbulent flow the more general definition of the collision-coalescence kernel

$$K(r_1, r_2) = 2\pi [r_1 + r_2]^2 w_r g_{12} E_{\text{coll}} \eta_E. \quad (2)$$

has to be used. Here w_r is the radial relative velocity at contact (~~Saffman and Turner, 1956~~) ([Saffman and Turner, 1956, 1988](#)). The radial distribution function g_{12} quantifies the effect of preferential concentration on the pair number density statistics and η_E represents an enhancement factor due to a modification of the collision efficiency by the turbulent flow. [For further details and explanations of the basic concepts we refer to the recent reviews by Devenish et al. \(2012\) and Grabowski and Wang \(2013\).](#)

Any physical model of w_r , g_{12} and η_E should be formulated in the dimensionless numbers that characterize the system. These are first of all the two Stokes numbers of the two colliding particles with the Stokes number being defined by

$$St = \frac{\tau_p}{\tau_k} \quad (3)$$

where τ_p is the particle relaxation time scale and τ_k is the Kolmogorov time scale. The particle relaxation time scale is given by

$$\tau_p = \frac{2}{9} \frac{\rho_p}{\rho_a} \frac{r^2}{\nu_a} \quad (4)$$

with the material density of the particle ρ_p (here liquid water with $\rho_p = 10^3 \text{ kg m}^{-3}$), the air density ρ_a and the kinematic viscosity of air ν_a . The Kolmogorov time scale τ_k is related to the Kolmogorov length scale ℓ_k and the turbulent dissipation rate ϵ by

$$\tau_k = \frac{\ell_k^2}{\nu_a} = \sqrt{\frac{\nu_a}{\epsilon}} \quad (5)$$

- 5 Due to the r^2 -dependency of τ_p the Stokes number increases with droplet size. Typical cloud droplets with radii smaller than 20 ~~μm~~ μm have Stokes number below 0.2, large cloud droplets and small rain drops are close to $St = 1$, while larger raindrops have large Stokes number $St \gg 1$. Preferential concentration effects, i.e., large values of g_{12} , occur for $St \approx 1$. Smaller droplets with smaller Stokes numbers simply follow the flow and show no clustering, while drops with $St \gg 1$ do not feel the small scale turbulence due to their inertia and their trajectories are, in addition, largely determined by their significant terminal fall
- 10 velocity. Therefore large cloud ~~droplet~~ droplets and small raindrops with radii between 20 and 100 ~~μm~~ μm are most strongly affected by turbulence effects.

A turbulent flow is not yet fully characterized by τ_k (or ϵ) alone. To quantify the root mean square of the turbulent velocity fluctuations, u_{rms} , we introduce the Taylor-microscale Reynolds number defined by

$$Re_\lambda = \frac{u_{rms} \lambda_T}{\nu_a} = \sqrt{15} \frac{\nu_a}{\epsilon} \frac{u_{rms}^2}{\nu_a}. \quad (6)$$

- 15 The Taylor-microscale Reynolds number is important for the collision statistics as it is closely related to the two-point correlation and the autocorrelation functions of turbulent flows. In general, turbulence has three independent length scales, the Kolmogorov scale, ℓ_k , the Taylor microscale, λ_T , and a large-eddy or integral length scale (Pope, 2000). Therefore we will throughout most of this paper treat ϵ and Re_λ as two independent variables. Only later when we apply the collision-coalescence model in LES we will parameterize Re_λ as a function of ϵ .

- 20 Various models have been suggested to parameterize w_r , g_{12} and η_E in terms of St and Re_λ . Here we focus on the models of Wang and Ayala (Ayala et al., 2008b, a; Wang et al., 2008; Wang and Grabowski, 2009) and Onishi (Onishi, 2005; Onishi et al., 2015). A detailed discussion of these two models has recently been given by Onishi and Seifert (2016). We refer to those papers for the relevant parameterization equations. Figure 1 shows the enhancement factor of the collision kernel due to turbulence effects, i.e., the ratio $K(r_1, r_2; \epsilon, Re_\lambda)/K_{\text{grav}}(r_1, r_2)$, for the Ayala-Wang and the Onishi model at $\epsilon = 1000 \text{ cm}^2 \text{ s}^{-3}$
- 25 for two different values of Re_λ .

- The Ayala-Wang model shows a significant increase of the collection kernel for high Reynolds numbers for droplet smaller than 80 μm radius, roughly a factor of 2 increase from $Re_\lambda = 1000$ to $Re_\lambda = 20000$ (Figs. 1a,b,c). For the Onishi kernel the Re_λ -dependency is more subtle and can be characterized as a shift of the maximum of the enhancement from smaller to larger droplets, i.e., the kernel decreases for small droplets ($r < 40 \mu\text{m}$) but increases for larger droplets ($r > 40 \mu\text{m}$) as the
- 30 Reynolds number increases. For an in-depth discussion of the Reynolds number dependencies we refer again to Onishi and Seifert (2016).

3 Parameterization of turbulence effects on autoconversion

~~For the~~ The evolution of the drop size distribution $f(x)$ as a function of drop mass x , where $f(x)dx$ is the number of drops per unit volume in the size range $[x, x + dx]$, is governed by the kinetic equation also known as the Smoluchowski coagulation equation (von Smoluchowski, 1916, 1917) which in its continuous form

$$\left. \frac{\partial f(x)}{\partial t} \right|_{\text{coag}} = \frac{1}{2} \int_0^x f(x-x') f(x') K(x-x', x') dx' - \int_0^\infty f(x) f(x') K(x, x') dx' \quad (7)$$

5 was first derived by Müller (1928). A detailed discussion of this equation and its mathematical properties is given in the classic review by Drake (1972) and more recently by da Costa (2015). Another classic, but still interesting contribution on the interpretation of the continuous form of the Smoluchowski equation is the paper by Gillespie (1975). Although various numerical methods are available to solve Eq. (7) directly (e.g. Berry and Reinhardt, 1974; Bott, 1998; Tzivion et al., 1999; Shima et al., 2000) this is most often seen as computationally too expensive in three-dimensional atmospheric models. Therefore bulk parameterizations are used which predict only a limited number of (partial) moments of the drop size distribution. Following Kessler (1969) and motivated by the emergence of bi-modal mass distributions as a consequence of the colloidal instability the size distribution is decomposed into two parts. Drops smaller than some threshold x^* are called cloud droplets, drops larger than x^* are called rain drops. The value of $x^* = 2.6 \times 10^{-10}$ kg which corresponds to a radius of $40 \mu\text{m}$ is not arbitrary but should be chosen as the local minimum of the bi-modal mass distribution function $g(x) = xf(x)$ during the colloidal instability (Beheng and Doms, 1986; Beheng, 2010). This minimum exists due to the properties of the (gravitational) coagulation kernel $K(x, y)$ which becomes less steep for $x > x^*$ (Long, 1974). Having defined the two drop categories, we can identify the following bulk microphysical processes: autoconversion is the formation of rain drops due to collisions between cloud droplets and accretion is the growth of rain drops due to the collection of cloud droplet by rain drops. The change of the number density within one category due to coagulation within this drop category is called selfcollection. For a more detailed review of the basic ideas of warm rain parameterizations we refer to the review of Beheng (2010). The increase in rain water content L_r due to autoconversion and accretion is given by the integrals (Doms and Beheng, 1986; Beheng and Doms, 1986; Beheng, 2010)

$$\left. \frac{\partial L_r}{\partial t} \right|_{\text{au}} = \frac{1}{2} \int_{x'=0}^{x^*} \int_{x''=x^*-x'}^{x^*} f(x') f(x'') K(x', x'') x' dx' \quad (8)$$

$$\left. \frac{\partial L_r}{\partial t} \right|_{\text{ac}} = \int_{x'=x^*}^{\infty} \int_{x''=0}^{x^*} f(x') f(x'') K(x', x'') x' dx'. \quad (9)$$

25 ~~For the~~ parameterization of autoconversion we follow Seifert and Beheng (2001, SB2001 hereafter). For a cloud droplet distribution which initially obeys a gamma distribution in particle mass x

$$f(x) = Ax^\nu e^{-Bx} \quad (10)$$

SB2001 derived the autoconversion parameterization

$$\left. \frac{\partial L_r}{\partial t} \right|_{\text{au}} = \frac{k_{cc}}{20x^*} \frac{(\nu+2)(\nu+4)}{(\nu+1)^2} L_c^2 \bar{x}_c^2 \left[1 + \frac{\Phi_{\text{au}}(\tau)}{(1-\tau)^2} \right]. \quad (11)$$

Here L_c is the cloud water content, $\bar{x}_c = L_c/N_c$ the mean cloud droplet mass with N_c being the cloud droplet number density, and $x^* = 2.6 \times 10^{-10} \text{ kg}$ is ~~is~~ is again the separating mass between cloud and rain drops. The dimensionless ratio $\tau = L_r/(L_c + L_r)$ with the rain water content L_r acts as an internal timescale and modulates the autoconversion rate due to the universal function $\Phi_{\text{au}}(\tau)$ given by

$$\Phi_{\text{au}}(\tau) = 600 \tau^{0.68} (1 - \tau^{0.68})^3. \quad (12)$$

In case of purely gravitational collection the kernel parameter for autoconversion is given by $k_{cc} = k_{cc,0} = 9.44 \times 10^9 \text{ s}^{-1} \text{ kg}^{-2}$ and originates from a piecewise polynomial approximation of the collection kernel (Long, 1974).

10 Following Seifert et al. (2010) we extend this autoconversion parameterization to include turbulence effects by making k_{cc} a function of ϵ , Re_λ and \bar{r}_c . The latter dependency is necessary, because the turbulence effects are different for droplets of different size. Seifert et al. (2010) have shown that the Ayala-Wang kernel can be approximated with the following ansatz

$$k_{cc}(\bar{r}_c, \nu, \epsilon, Re_\lambda) = k_{cc,0} \left\{ 1 + \epsilon Re_\lambda^p \left[\alpha_{cc}(\nu) \exp \left\{ - \left[\frac{\bar{r}_c - r_{cc}(\nu)}{\sigma_{cc}(\nu)} \right]^2 \right\} + \beta_{cc} \right] \right\} \quad (13)$$

where

$$15 \quad \alpha_{cc}(\nu) = \frac{a_1 + a_2 \nu}{1 + a_3 \nu} \quad (14)$$

$$r_{cc}(\nu) = \frac{b_1 + b_2 \nu}{1 + b_3 \nu} \quad (15)$$

$$\sigma_{cc}(\nu) = \frac{c_1 + c_2 \nu}{1 + c_3 \nu} \quad (16)$$

20 are functions of the shape parameter ν only. Here we use the same ansatz for the updated Ayala-Wang kernel and for the Onishi kernel. The 11 coefficients of this model have been determined by a nonlinear least square fit using a data base of numerical solutions of the stochastic collection equation (SCE). The parameter space covered by the SCE simulations is $\epsilon \in [0, 1000] \text{ cm}^2 \text{ s}^{-3}$, $Re_\lambda \in [1000, 25000]$, $L_c \in [0.2, 2] \text{ g m}^{-3}$, $\bar{r}_c \in [8, 20] \mu\text{m}$ and $\nu \in [0, 4]$. Note that in contrast to Seifert et al. (2010) we have extended the range for ϵ to values up to $1000 \text{ cm}^2 \text{ s}^{-3}$ to allow for the higher dissipation rates that occur, for example, in
25 cumulus congestus. The resulting coefficients for both turbulence kernels are given in Table 1.

The most notable difference between the two kernels is that for the Ayala-Wang kernel the autoconversion rate increases with Re_λ resulting in $p = 1/4$, whereas autoconversion decreases slowly with increasing Re_λ for the Onishi kernel with a power law exponent $p = -1/8$. ~~The~~

The different autoconversion enhancement factors for the two kernels and the quality of the fits is ~~confirmed~~ shown by Fig. 2 a,b and in which also the Reynolds number dependency is shown in more detail in Fig. 2c. The latter reveals that ~~the~~. The results for the Ayala-Wang kernel show somewhat higher enhancement factors compared to Seifert et al. (2010), mostly due to the improved treatment of the collision efficiency (cf. Onishi and Seifert, 2016). The Onishi kernel shows much lower enhancement factors and the maximum is shifted to larger (mean) droplet radii compared to the Ayala-Wang kernel. The Re_λ -dependency reveals that especially for the Onishi kernel the value of the exponent, $p = -1/8$, is really just a fit with limited physical meaning as the actual slope has significant dependencies on \bar{r}_c and Re_λ . This more complicated behavior is consistent with the analysis presented by Onishi and Seifert (2016) who showed that the Reynolds number dependency of the kernel varies with Stokes number (e.g. their Figure 2). For the Ayala-Wang kernel the numerical data shows a slightly steeper increase with Re_λ compared to the parameterization. This is mostly because we kept to exponent at $p = 1/4$ as in Seifert et al. (2010), although the extended range of the dissipation rate in the current study would ask for a slightly higher exponent. The dependency on dissipation rate is assumed to be linear in Eq. (13) and this is confirmed for the Onishi kernel, but for the Ayala-Wang kernel the ϵ -dependency becomes slightly weaker for high dissipation rates.

A first test of the autoconversion parameterization is obtained by simulations of exactly the same kind as used as training data, i.e., SCE simulations with an initial condition following a gamma distribution. As a metric for evaluation with use the time scale t_{10} which is defined as the time needed to convert 10 % of the initial liquid water to rain water. Figure 3 shows the dependencies of t_{10} on dissipation rate ϵ , initial mean drop radius \bar{r}_c and initial cloud water content L_c . This confirms that the fit is reasonable and that the autoconversion parameterization captures those dependencies correctly.

4 Turbulence effects in a 1D kinematic model

As in Seifert et al. (2010) we use the 1D kinematic model of Seifert and Stevens (2010) as a slightly more complete test problem for the warm rain scheme. The 1D kinematic model is especially useful as it describes the various stages of the warm rain formation in an isolated cumulus cloud. This is necessary to test and validate our assumptions regarding accretion and selfcollection of raindrops. Those two processes depend strongly on drop sedimentation and the resulting drop size distribution and can therefore hardly be tested in pure SCE simulations. Although the 1D model provides a reasonable idealized framework for such a test, we would recommend to use a kinematic 2D model (e.g. Szumowski et al., 1998; Morrison and Grabowski, 2007) in future studies, because the 1d framework might not be sensitive enough to differences in the treatment of sedimentation which are more relevant in a more complex flow field. Here we apply the simpler 1D model for consistency with Seifert et al. (2010).

~~As in Seifert et al. (2010) we use the enhancement factor~~

$$k_{rr} = k_{cr,0} (1 + \hat{c}_r \epsilon^{\frac{1}{4}})$$

with $\hat{c}_r = 0.05 \text{ cm}^{-1/2} \text{ s}^{3/4}$ for accretion. The accretion rate and selfcollection of rain when using are parameterized as

$$\left. \frac{\partial L_r}{\partial t} \right|_{ac} = k_{cr} L_c L_r \Phi_{ac}(\tau) \eta_{ac} \quad \text{with} \quad \Phi_{ac} = \left(\frac{\tau}{\tau + 5 \times 10^{-4}} \right)^4 \quad (17)$$

and

$$\left. \frac{\partial N_r}{\partial t} \right|_{sc} = -k_{rr} N_r L_r \eta_{sc} \quad (18)$$

- 5 with $k_{cr} = 5.78 \text{ m}^3 \text{ kg}^{-1} \text{ s}^{-1}$ and $k_{rr} = 4.33 \text{ m}^3 \text{ kg}^{-1} \text{ s}^{-1}$ and turbulent enhancement factors η_{ac} and η_{sc} . In case of the Ayala-Wang kernel we use the same enhancement factors as in Seifert et al. (2010) with

$$\eta_{ac} = \eta_{sc} = 1 + \hat{c}_r \epsilon^{\frac{1}{4}} \quad (19)$$

with $\hat{c}_r = 0.05 \text{ cm}^{-1/2} \text{ s}^{3/4}$. For the Onishi kernel we apply a stronger enhancement which is linear in the dissipation rate ϵ

$$\eta_{ac} = \eta_{sc} = 1 + \check{c}_r \epsilon \left(\frac{x^*}{\bar{x}_r} \right)^{\frac{2}{3}} \quad (20)$$

- 10 with $\check{c}_r = 0.8 \times 10^{-3} \text{ cm}^{-2} \text{ s}^3$. For a dissipation rate of $1000 \text{ cm}^2 \text{ s}^{-3}$ this corresponds to an increase in accretion of 28 % in case of the Ayala-Wang kernel and 80 % for the Onishi kernel. For the Onishi kernel we have included an additional dependency on $\bar{x}_r \bar{x}_r = L_r / N_r$ to suppress the turbulent enhancement for very large (mean) raindrop sizes that do not feel the effect of small-scale turbulence. The enhancement factors for accretion and selfcollection cannot be directly derived from the collection kernel alone. The turbulent enhancement of the collision rate leads also to changes in the drop size distribution, i.e., the increase
- 15 in accretion and selfcollection is attributed, first, to the direct increase in the collision rates by the local turbulence and, second, to a modification of the drop size distribution by the turbulence effect. The latter constitutes a memory effect and makes it also difficult to discuss the turbulence effects on accretion and selfcollection separately, because these two processes are strongly linked. In the following we always mean the combined action of selfcollection of rain and accretion, when we discuss effects of turbulence on the droplet growth by accretion.

- 20 Extensive test with the 1D kinematic model have shown that the parameterization compares reasonably well with the bin microphysics solution for both collection kernels. The most important metric to evaluate the warm rain scheme in the 1D kinematic model is the precipitation amount at the surface. One could argue that the timing is almost as relevant as the precipitation amount, but as shown by Seifert and Stevens (2010) the precipitation efficiency in the 1D cloud model depends mostly on the time scales of dynamics and microphysics, respectively their ratio, the Damköhler number. Therefore we discuss here only the
- 25 precipitation amounts which are presented in Figure 4 as a function of dissipation rate (which is assumed as homogeneous within the cloud) for two different Reynolds numbers and various aerosol number concentrations N_a . For further details, e.g., on the treatment of activation we refer to Seifert and Stevens (2010). For the Ayala-Wang kernel we find a significant increase in surface precipitation, for example, we find an increase by a factor of 2 for low N_a (clean conditions) when ϵ is as large as $1000 \text{ cm}^2 \text{ s}^{-3}$ compared to pure gravitational kernel ($\epsilon = 0$). For high N_a the cloud does not produce any rain without the

effect of turbulence on the collision rate ($\epsilon = 0$), but yields significant rain when turbulence can contribute to rain formation. For the Onishi kernel we find qualitatively the same behavior, but the rain amounts are significantly lower especially for low dissipation rates ϵ . The different Reynolds number dependencies of both kernels are also visible in these surface rain amounts. For the Ayala-Wang kernel the rain amounts increase significantly for higher Reynolds numbers. In case of the Onishi kernel a slight decrease is observed for high N_a when increasing Re_λ from 1000 to 20000. For $N_a = 50 \text{ cm}^{-3}$ a slight increase with Re_λ is visible for the spectral model, but not for the two-moment scheme. This can be attributed to the increase in the accretion rate in the Onishi kernel for high Re_λ and this effect we have neglected in the bulk scheme (mostly because the Re-dependency is quite weak and in addition the low Re_λ case is not important for cloud physics applications). Nevertheless, the 1D kinematic model suggests that the turbulence effect on accretion is significant, and even more so in case of the Onishi kernel. Especially for low N_a , when autoconversion is quite efficient, accretion can become the limiting process for droplet growth and an increase in accretion due to turbulence effects can significantly affect surface rain amount. This will be further investigated using large-eddy simulations in the following section.

5 Turbulence effects in large-eddy simulations of trade wind cumuli

5.1 Model setup

To investigate the effect of in-cloud turbulence on rain formation in trade wind cumulus clouds we perform large-eddy simulations of the Rain In Cumulus over the Ocean (RICO) case as described by van Zanten et al. (2011). We use the standard RICO case and not the moister initial condition ~~of~~ as in Seifert et al. (2010). We apply the UCLA-LES model (Stevens et al., 2005; Stevens, 2007) on a domain of $51.2 \text{ km} \times 51.2 \text{ km}$ with doubly-periodic boundary conditions, a simulation time of at least 30 h and a horizontal mesh size of 50 m with additional simulations at finer and coarser grid spacing. The model time step is variable with a maximum Courant number below 0.5. The time step is mostly dominated by the vertical grid spacing and velocity and approximately 1 s. The cloud microphysical parameterization follows SB2001 and Stevens and Seifert (2008) with the modifications described in the previous sections. For the shape parameter of the cloud droplet size distribution we use $\nu = 1$ in all simulations. The sub-grid scale (SGS) turbulence model is a Smagorinsky-Lilly closure including a proper treatment of anisotropic grids (Scotti et al., 1993). As described in detail in Seifert et al. (2010) the SGS models provides the local (grid point) turbulent dissipation rate ϵ which is needed for the turbulence effect on cloud microphysics. Additional assumptions are necessary for the Reynolds number Re_λ as the SGS model does neither provide Re_λ nor u_{rms} . Here we follow Wyszogrodzki et al. (2013) and parameterize Re_λ as a function of ϵ alone. Consistent with homogeneous isotropic turbulence we use the scaling relation $Re_\lambda = Re_0(\epsilon/\epsilon_0)^{1/6}$ with $Re_0 = 10000$ and $\epsilon_0 = 100 \text{ cm}^2 \text{ s}^{-3}$.

5.2 Turbulence effect on rain formation

Figure 5 shows time series from a first set of simulations with grid spacing $\Delta x = 50 \text{ m}$. After some initial spin up the cloud liquid water path increases slowly with time corresponding to a slowly deepening cloud layer. Rain water develops after a

few hours and surface precipitation is observed subsequently. The rain water path, surface rain rate and the timing of the rain formation differs strongly between the various simulations. The control simulation which uses the purely gravitational kernel develops only marginal rain and surface precipitation within the 30 h period. In contrast, the simulation which applies the Ayala-Wang kernel develops rain much earlier and the rain rate reaches 1 mm/d after about 20 h with some fluctuations later-on. Using the Onishi kernel leads to faster rain formation compared to the control simulations, but slower than for the Ayala-Wang kernel. At the end of the simulation period the Onishi kernel yields similar rain rates as the Ayala-Wang kernel, i.e., in the last hours both turbulence kernels increase the surface rain rate by a factor 7 relative to the control run. Especially for the Onishi kernel the enhancement of the rain formation is due to the combined action of the increased autoconversion and accretion. This is illustrated by an additional simulation which uses only the enhancement for autoconversion, but ignores the effect on accretion. The resulting time series are much closer to the control run and show only a significant increase in rain rate at the very end of the simulation period. This underpins our results of the previous section that the rain formation in shallow cumulus clouds is not only limited by autoconversion, but also by accretion. Although accretion increases more strongly in the Onishi kernel than in the Ayala-Wang kernel, the LES results show that this can not compensate for the weaker increase in autoconversion resulting in a reduced turbulence effect on rain formation. The [main feedback of the different microphysical developments on the dynamics and the evolution of the boundary layer as a whole is that rain formation arrests the growth of the cloud layer as it can be seen in the time series of the inversion height in Fig. 5, i.e., the Ayala-Wang kernel leads to a much shallow cloud layer in the precipitating regime. A similar behavior for different cloud droplet number densities was shown by Stevens and Seifert \(2008\) and \(Seifert et al., 2015\). For the RICO case the boundary layer deepens and supports successively deeper clouds until moisture is efficiently removed by precipitation. Eventually the precipitating regime reaches a quasi-stationary state, the subsiding radiative-convective equilibrium \(Seifert et al., 2015\).](#)

The strong turbulence effect of both kernels suggested by Figure 5 is consistent with Seifert et al. (2010) and Wyszogrodzki et al. (2013), but two important aspects have to be considered. First, this behavior is transient, i.e., even the purely gravitational case would develop significant rain of order 1 mm/d after some time. Extending the simulation further shows that this happens after about 35 h. Second, Fig. 5 shows only simulations for a specific intermediate value of the cloud droplet number density. A lower value will make rain formation easier and more efficient also for the gravitational kernel and lead to smaller differences, a higher droplet number may suppress precipitation even for the collection kernels that include turbulence effects. To get a more complete picture we have to discuss both effects.

5.3 Sensitivity to cloud droplet number

We have performed a larger set of large-eddy simulations for different cloud droplet number densities. In addition, simulations have been repeated with different random seeds to sample the stochastic uncertainty of the system and to reduce the standard error in the statistical evaluation. Table 2 summarizes the results in terms of domain-mean statistical quantities like cloud cover, inversion height, rain water path, etc. As a measure for the temporal, i.e., transient behavior we have calculated two time scales that characterize the rain formation by the exceedance of thresholds for the domain-averaged rain rate, t_1 for a threshold of 0.1 mm/d and t_2 for 0.8 mm/d. While t_1 measures the first occurrence of rain at the surface, the larger threshold

value of t_2 characterizes the transition to organized precipitation shallow convection (Seifert et al., 2015). The most important results are summarized in Fig. 6 which illustrates the turbulence effects on the rain formation for different values of the cloud droplet number density. Shown are domain-mean quantities from 24 h to 30 h of the simulations and standard error is depicted by shaded areas. The standard error is estimated as σ_x/n_x where σ_x is the standard deviation of that variable and n_x is its effective sample size. For each simulation we estimate the effective sample size during the sampling period of 6 hours as $n_x = n_0(1 - r_1)/(1 + r_1)$ where r_1 is the lag-1 autocorrelation and n_0 is the number of samples in the time series. This simple formulation gives almost the same results as a more sophisticated implementation following Zwiers and von Storch (1995). As shown in Fig. 6 rain water path and surface rain rate increase with decreasing cloud droplet number, but also show a pronounced impact of turbulence-induced collisions. For $N_c = 50 \text{ cm}^{-3}$, i.e., the simulations which are also shown in Fig. 5, both the Ayala-Wang kernel and the Onishi kernel lead to a strong increase in RWP and rain rate. For the lower value of $N_c = 35 \text{ cm}^{-3}$ the purely gravitational kernel used in the control simulations is sufficient to produce similar values of RWP and rain rate and the differences between the three kernels are no longer statistically significant. For an increase in droplet number the rain formation gets suppressed. Already for $N_c = 70 \text{ cm}^{-3}$ the rain rate and RWP for the Onishi kernel drops to values which are hardly different from the purely gravitational case, while the Ayala-Wang kernel still shows a strong enhancement leading to rain rates of order 1 mm/d during the 30 h period. Finally, for $N_c = 105 \text{ cm}^{-3}$ the rain formation starts to get suppressed even for the Ayala-Wang kernel and for droplet number exceeding that value all three collection kernels would only yield marginal precipitation within the 30 h period.

For low cloud droplet numbers we do not find a significant difference for the rain water path and the surface rain rate between the three different kernel during the 24 h to 30 h sampling period, because all three simulations develop a rain rate that is close to the quasi-equilibrium rain water flux. Nevertheless, the transient behavior is different between the three kernels for all droplet number densities as, e.g., seen from the time scales t_1 and t_2 in Figure 7. The Ayala-Wang kernel leads to an acceleration of the rain formation by more than 10 h for high drop number and still several hours for low droplet numbers. The acceleration caused by the Onishi kernel is less strong and becomes smaller for t_2 for low drop numbers while the difference in t_1 to the control run remains also for low drop numbers. This difference in the transient behavior leaves an imprint in the structure of the boundary layer even for long simulation times in the sense that the Ayala-Wang kernel, which develops rain most easily, arrests to growth of the boundary layer much earlier leading to the lowest inversion height in the precipitating regime (Fig. 6c). For the Onishi kernel this cloud macroscopic effect of the microphysical processes is much weaker. That the cloud droplet number and the microphysical efficiency of the cumulus clouds modulates the inversion height is consistent with the results of Stevens and Seifert (2008) and Seifert et al. (2015).

The turbulence effects on the collision rate, as postulated by the two different turbulence models, lead to a strong increase of the autoconversion rate and a moderate increase of accretion. This is true for both kernels, although the Onishi model has a weaker enhancement of autoconversion and a stronger increase in accretion, especially at high Reynolds numbers. It is therefore interesting to check whether a significant shift in the importance of those two warm rain processes can be observed in the large-eddy simulations. Figure 6d shows the ratio of accretion over autoconversion, AC/AU , for the sampling period of 24 h to 30 h. For all simulations accretion is the dominant process and total accretion exceeds autoconversion by a factor

of 3 or more. Interestingly, the simulations which take into account turbulence effects show a higher AC/AU -ratio compared to the control simulations, which is counter-intuitive as the enhancement mostly affects autoconversion. This behavior can be understood from the relation between autoconversion and accretion. A higher autoconversion rate will most likely lead to a subsequent increase in accretion, because more small rain drops become available for accretional growth. Therefore an increase in the autoconversion rate, as caused by the turbulence effects, has little effect on the AC/AU -ratio. In fact, the higher rain rate regimes of the simulations with the turbulence kernels favor accretion over autoconversion. Therefore the observed AC/AU -ratio is not directly linked to the turbulent enhancement factors of the process rates.

5.4 Sensitivity to grid resolution

Previous studies, e.g., by Matheou et al. (2011) and Seifert and Heus (2013) have emphasized that especially the precipitating RICO case exhibits a strong sensitivity to the grid spacing used in large-eddy simulations. We have therefore performed another set of simulations to test the sensitivity to grid spacing using 100 m, 50 m and 25 m horizontal mesh size for the three different collection kernels. The vertical grid spacing for all simulations is fixed at 25 m. Figure 8 summarizes the main results of the resolution study. The detailed statistics of the individual simulations are given in Table 3. For cloud liquid water path hardly any sensitivity to grid spacing is found, but the simulations with the Ayala-Wang kernel lead in general to a reduced CWP. This can be explained by the more rapid conversion of cloud water to rain, and by the shallower cloud layer in the precipitating regime. For rain water path and surface rain rate we find a strong increase with increasing resolution for the Onishi kernel and the control simulations. At 25 m grid spacing all three models give similar RWP and surface rain rate and differences are not statistically significant for those two variables. This is a similar behavior as for the reduced cloud droplet number. A small grid spacing in the LES makes the rain formation more rapid and the differences between the kernels becomes smaller when they all reach the precipitating regime before the chosen sampling period. This is confirmed by Fig. 9 which shows that the time scale t_2 decreases with resolution and at 25 m grid spacing all three kernels have a t_2 smaller than 20 h, i.e., the sampling period of 24 h to 30 h is in the precipitating regime for all three collision kernels. Figs. 8 and 9 reveal that the LES is not yet converged even at 25 m grid spacing. Unfortunately, higher resolution than the 25 m grid becomes very expensive and cannot be tested here. Differences in inversion height remain present even at the highest resolution, especially the Ayala-Wang kernel leads to much shallower cloud layers. A hint towards the causes of the strong resolution dependency is maybe given by the AC/AU -ratio which increases strongly for higher resolution. Especially the control run exhibits a significant increase from below 4 at 50 m grid spacing to almost 8 at 25 m. The rain efficiency, defined as the ratio of evaporation of rain over the sum of autoconversion and accretion, $1 - EV/(AU + AC)$, shows a behavior very similar to the AC/AU -ratio and suggests that the growth by accretion leads to large raindrops which are less susceptible to evaporation, thus more rain reaching the ground. The strong sensitivity of the rain formation to grid spacing may be surprising at first as individual precipitating cumulus clouds have horizontal scales of at least 1000 m and should be well resolved by the LES already at 50 m grid spacing. We suggest two possible mechanisms to explain the observed sensitivity. First, due to the strong nonlinearity of the autoconversion rate small scale fluctuations in cloud water may trigger autoconversion earlier and more often and initiate the rain formation more effectively at high resolution. Second, the in-cloud circulations which are better resolved at higher resolution increase the in-

cloud residence time of the rain drops and therefore their overall growth by selfcollection and accretion. The latter effect has recently been emphasized as an important growth mechanism for raindrops in shallow cumulus clouds (Naumann and Seifert, 2016). Although it remains questionable whether a two-moment bulk scheme can represent recirculation properly, the strong increase of accretion observed in Fig. 8d would favor the second explanation. Whatever the detailed mechanism is, the strong
5 sensitivity to grid spacing suggests that the larger modes of turbulence, like turbulent entraining eddies, which are resolved by high-resolution LES, play an important role in enhancing the rain formation. This provides a second mechanism in addition to the effect of the small-scale isotropic turbulence on collision rates which is parameterized by the Ayala-Wang or Onishi kernel and sub-grid for any LES model.

6 Conclusions

10 We have derived a warm rain bulk two-moment scheme which incorporates the effects of small-scale isotropic turbulence on the collision rate following the two alternative models of Ayala-Wang and Onishi. The two collision kernels differ mostly in their Reynolds number dependency. While the Ayala-Wang model postulates an increase of autoconversion with Reynolds number, the Onishi model predicts a decrease of autoconversion, but an increase in accretion for high Reynolds number. The two newly derived variants of the Seifert-Beheng warm rain scheme have been tested and validated in 1D simulations and
15 compare favorably with the bin microphysics model that acts as a reference.

The new bulk scheme has been applied in large-eddy simulations of precipitating shallow convection to investigate the impact of the different collision kernels. Both turbulence kernels lead to a significant enhancement of the rain formation in shallow convective clouds, but the turbulence effect is much weaker for the Onishi kernel. Especially for intermediate cloud droplet numbers, in our simulations 50 cm^{-3} but this might differ from case to case, the turbulence enhancement can lead to
20 a strong increase in rain water path and surface rain rate compared to a purely gravitational collection kernel. For the Ayala-Wang kernel we find a significant reduction of the height of the trade wind inversion, because the rapid rain formation arrests to growth of the cloud layer. This effect is not significant for the Onishi kernel.

The large-eddy simulations show a strong sensitivity to horizontal grid spacing with a more rapid rain formation at higher resolution. This suggests that the larger turbulent eddies like in-cloud circulations, which are resolved by high-resolution LES,
25 can play an important role for the growth of rain drops. It is hypothesized that rain drops with large Stokes numbers, $St > 1$, can interact with these large turbulent eddies. For example, in the two-moment bulk scheme used in the present study such effects are not yet accurately parameterized and need to be investigated in more detail in future studies.

Our results show that the differences between the Ayala-Wang model and the Onishi models are significant and it needs to be clarified either by observations or by additional DNS studies which collision kernel is more realistic at high Reynolds numbers.

30 *Acknowledgements.* We thank the computing center of ECWMF where all simulations were performed using resources provided through DWD. We thank Ann Kristin Naumann for helpful comments on the manuscript. [We thank the three anonymous reviewers for their comments that helped to improve the manuscript.](#) The UCLA-LES model is distributed under GNU General Public License and can easily be down-

loaded from <https://github.com/uclales>. Model code and input files necessary to reproduce the specific experiments of this study, are available from the corresponding author upon request.

References

- Ayala, O., Rosa, B., and Wang, L.-P.: Effects of turbulence on the geometric collision rate of sedimenting droplets. Part 2. Theory and parameterization, *New Journal of Physics*, 10, 075 016 (40pp), 2008a.
- Ayala, O., Rosa, B., Wang, L.-P., and Grabowski, W.: Effects of turbulence on the geometric collision rate of sedimenting droplets. Part 1. Results from direct numerical simulation, *New Journal of Physics*, 10, 075 015 (31pp), 2008b.
- 5 Beard, K. V. and Ochs, H. T.: Warm-Rain Initiation: An Overview of Microphysical Mechanisms, *J. Appl. Met.*, 32, 608–625, 1993.
- Beheng, K. D.: The evolution of raindrop spectra: A review of basic microphysical essentials, *Rainfall: State of the Science*, Geophys. Monogr., 191, 29–48, 2010.
- Beheng, K. D. and Doms, G.: A general formulation of collection rates of cloud and raindrops using the kinetic equation and comparison with parameterizations, *Contrib. Atmos. Phys.*, 59, 66–84, 1986.
- 10 Berry, E. X. and Reinhardt, R. L.: An Analysis of Cloud Drop Growth by Collection: Part I. Double Distributions, *J. Atmos. Sci.*, 31, 1814–1824, 1974.
- Bott, A.: A Flux Method for the Numerical Solution of the Stochastic Collection Equation, *J. Atmos. Sci.*, 55, 2284–2293, 1998.
- da Costa, F.: Mathematical Aspects of Coagulation-Fragmentation Equations, in: *Mathematics of Energy and Climate Change*, edited by Bourguignon, J.-P., Jeltsch, R., Pinto, A. A., and Viana, M., pp. 83–162, Springer International Publishing, doi:10.1007/978-3-319-16121-1_5, 2015.
- 15 Devenish, B. J., Bartello, P., Brenguier, J.-L., Collins, L. R., Grabowski, W. W., IJzermans, R. H. A., Malinowski, S. P., Reeks, M. W., Vassilicos, J. C., Wang, L.-P., and Warhaft, Z.: Droplet growth in warm turbulent clouds, *Quart. J. Roy. Met. Soc.*, 138, 1401–1429, doi:10.1002/qj.1897, 2012.
- 20 Doms, G. and Beheng, K. D.: Mathematical formulation of self-collection, autoconversion and accretion rates of cloud and raindrops, *Meteorol. Rdsch.*, 39, 98–102, 1986.
- Drake, R.: A general mathematical survey of the coagulation equation, in: *Topics in current aerosol research*, edited by Hidy, G. and Brock, J., pp. 201–376, Pergamon Press, Oxford, 1972.
- Gillespie, D. T.: Three models for the coalescence growth of cloud drops, *J. Atmos. Sci.*, 32, 600–607, 1975.
- 25 Grabowski, W. and Wang, L.-P.: Growth of cloud droplets in a turbulent environment, *Annu. Rev. Fluid Mech.*, 45, 293–324, doi:10.1146/annurev-fluid-011212-140750, 2013.
- Kessler, E.: On the distribution and continuity of water substance in atmospheric circulations, *Meteor. Monogr.* 32, Amer. Meteor. Soc., Boston, 1969.
- Long, A. B.: Solutions to the droplet collection equation for polynomial kernels, *J. Atmos. Sci.*, 31, 1040–1052, 1974.
- 30 Matheou, G., Chung, D., Nuijens, L., Stevens, B., and Teixeira, J.: On the Fidelity of Large-Eddy Simulation of Shallow Precipitating Cumulus Convection, *Mon. Wea. Rev.*, 139, 2918–2939, 2011.
- Morrison, H. and Grabowski, W. W.: Comparison of Bulk and Bin Warm-Rain Microphysics Models Using a Kinematic Framework, *J. Atmos. Sci.*, 64, 2839–2861, doi:10.1175/JAS3980, 2007.
- Müller, H.: Zur allgemeinen Theorie der raschen Koagulation, *Kolloidchem. Beihefte*, 27, 223–250, 1928.
- 35 Naumann, A. K. and Seifert, A.: Recirculation and growth of raindrops in simulated shallow cumulus, *J. Adv. Model. Earth Syst.*, pp. n/a–n/a, doi:10.1002/2016MS000631, 2016.

- Onishi, R.: Numerical simulations of chemical reaction and droplet growth in environmental turbulent flows, Ph.D. thesis, Kyoto University, 2005.
- Onishi, R. and Seifert, A.: Reynolds number dependence of turbulence enhancement on collision growth, *Atmos. Chem. Phys. Discuss.*, in review, doi:10.5194/acp-2016-19, 2016.
- 5 Onishi, R., Matsuda, K., and Takahashi, K.: Lagrangian Tracking Simulation of Droplet Growth in Turbulence-Turbulence Enhancement of Autoconversion Rate, *J. Atmos. Sci.*, 72, 2591–2607, doi:10.1175/JAS-D-14-0292.1, 2015.
- Pope, S. B.: *Turbulent flows*, Cambridge University Press, 2000.
- Pruppacher, H. R. and Klett, J. D.: *Microphysics of Clouds and Precipitation*, Kluwer Academic Publishers, Dordrecht, 1997.
- Saffman, P. G. and Turner, J. S.: On the collision of drops in turbulent clouds, *J. Fluid Mech.*, 1, 16–30, 1956.
- 10 Saffman, P. G. and Turner, J. S.: Corrigendum: On the collision of drops in turbulent clouds., *J. Fluid Mech.*, 196, 599, 1988.
- Scotti, A., Meneveau, C., and Lilly, D.: Generalized Smagorinsky model for anisotropic grids, *Phys. of Fluids A*, 5, 2306–2308, 1993.
- Seifert, A. and Beheng, K. D.: A double-moment parameterization for simulating autoconversion, accretion and selfcollection, *Atmos. Res.*, 59-60, 265–281, 2001.
- Seifert, A. and Heus, T.: Large-eddy simulation of organized precipitating trade wind cumulus clouds, *Atmos. Chem. Phys.*, 13, 5631–5645, 15 2013.
- Seifert, A. and Stevens, B.: Microphysical scaling relations in a kinematic model of isolated shallow cumulus clouds, *J. Atmos. Sci.*, 67, 1575–1590, 2010.
- Seifert, A., Nuijens, L., and Stevens, B.: Turbulence effects on warm-rain autoconversion in precipitating shallow convection, *Quart. J. Roy. Met. Soc.*, 136, 1753–1762, 2010.
- 20 Seifert, A., Heus, T., Pincus, R., and Stevens, B.: Large-eddy simulation of the transient and near-equilibrium behavior of precipitating shallow convection, *J. Adv. Model. Earth Syst.*, doi:10.1002/2015MS000489, 2015.
- Shima, S., Kusano, K., Kawano, A., Sugiyama, T., and Kawahara, S.: The super-droplet method for the numerical simulation of clouds and precipitation: a particle-based and probabilistic microphysics model coupled with a non-hydrostatic model, *Quart. J. Roy. Met. Soc.*, 135, 1307–1320, doi:10.1002/qj.441, 2009.
- 25 Stevens, B.: On the Growth of Layers of Non-precipitating Cumulus Convection, *J. Atmos. Sci.*, 64, 2916–2931, 2007.
- Stevens, B. and Seifert, A.: Understanding macrophysical outcomes of microphysical choices in simulations of shallow cumulus convection, *J. Met. Soc. Jap.*, 86, 143–162, 2008.
- Stevens, B., Moeng, C., Ackerman, A., Bretherton, C., Chlond, A., de Roode, S., Edwards, J., Golaz, J., Jiang, H., Khairoutdinov, M., Kirkpatrick, M., Lewellen, D., Lock, A., Muller, F., Stevens, D., Whelan, E., and Zhu, P.: Evaluation of large-Eddy simulations via 30 observations of nocturnal marine stratocumulus, *Mon. Wea. Rev.*, 133, 1443–1462, 2005.
- Szumowski, M. J., Rauber, R. M., Ochs III, H. T., and Beard, K. V.: The Microphysical Structure and Evolution of Hawaiian Rainband Clouds. Part II: Aircraft Measurements within Rainbands Containing High Reflectivity Cores, *J. Atmos. Sci.*, 55, 208–226, 1998.
- Tzivion, S., Reisin, T. G., and Levin, Z.: A Numerical Solution of the Kinetic Collection Equation Using High Spectral Grid Resolution: A Proposed Reference, *J. Comp. Phys.*, 148, 527–544, 1999.
- 35 van Zanten, M., Stevens, B., Nuijens, L., Siebesma, A., Ackerman, A., Burnet, F., Cheng, A., Couvreux, F., Jiang, H., Khairoutdinov, M., Kogan, Y., Lewellen, D., Mechem, D., Nakamura, K., Noda, A., Shipway, B., Slawinska, J., Wang, S., and Wyszogrodzki, A.: Controls on precipitation and cloudiness in simulations of trade-wind cumulus as observed during RICO, *J. Adv. Model. Earth Syst.*, 3, 2011.

- von Smoluchowski, M.: Drei Vorträge über Diffusion, Brownsche Molekularbewegung und Koagulation von Kolloidteilchen, *Physik. Zeitschr.*, 17, 557–599, 1916.
- von Smoluchowski, M.: Versuch einer mathematischen Theorie der Koagulationskinetik kolloidaler Lösungen, *Z. Phys. Chem.*, 92, 129–168, 1917.
- 5 Wang, L.-P. and Grabowski, W.: The role of air turbulence in warm rain initiation, *Atmos. Sci. Let.*, 10, 1–8, 2009.
- Wang, L.-P., Ayala, O., Rosa, B., and Grabowski, W.: Turbulent collision efficiency of heavy particles relevant to cloud droplets, *New Journal of Physics*, 10, 075 013 (41pp), 2008.
- Wyszogrodzki, A. A., Grabowski, W. W., Wang, L.-P., and Ayala, O.: Turbulent collision-coalescence in maritime shallow convection, *Atmos. Chem. Phys.*, 13, 8471–8487, doi:10.5194/acp-13-8471-2013, 2013.
- 10 Zwiers, F. W. and von Storch, H.: Taking Serial Correlation into Account in Tests of the Mean, *Journal of Climate*, 8, 336–351, 1995.

Table 1. Coefficients as a result of the nonlinear regression for k_{cc} as given by Eqs. (13)-(16).

	Ayala-Wang	Onishi	Unit
p	1/4	-1/8	-
a_1	7.432×10^{-4}	3.985×10^{-3}	cm^{-2}s^3
a_2	-6.993×10^{-5}	6.210×10^{-3}	cm^{-2}s^3
a_3	-9.497×10^{-2}	1.331	-
b_1	10.73	13.81	μm
b_2	13.56	9.980	μm
b_3	1.005	0.5018	-
c_1	6.607	6.325	μm
c_2	2.547	-0.9238	μm
c_3	0.2350	-0.1528	-
β_{cc}	3.480×10^{-4}	2.026×10^{-3}	cm^{-2}s^3

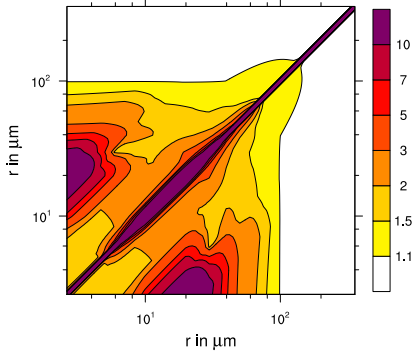
Table 2. Statistics for the large-eddy simulations assuming different collection kernel. N_x is the number of grid point in the horizontal, Δx and Δz are the horizontal and vertical grid spacing. Listed variables are the time scales t_1 and t_2 which characterize the transition to precipitating shallow convection (0.1 mm/d as rain rate-threshold for t_1 , 0.8 mm/d for t_2 , the area-averaged cloud cover C , the inversion height z_i , cloud liquid water path CWP in g/m^2 , rain water path RWP in g/m^2 , surface rain rate R in W m^{-2} (29 W m^{-2} corresponds to mm d^{-1}). The ratio of accretion over autoconversion, AC/AU , and the rain efficiency, $RE = 1 - EV/(AU + AC)$ (both evaluated over the whole column). Time averages are from 24 h to 30 h. The simulations shown in Fig. 5 are indicated by a grey background. Simulations with identical model configuration (kernel, N_x , Δx , Δz , N_c) differ only by the random seed of the initial condition.

n	kernel	N_x	Δx	Δz	N_c	t_1	t_2	C	z_i	CWP	RWP	R	AC/AU	RE
1	no turb.	1024	50	25	35.0	7.5	21.6	16.7	2238	12.6	17.3	43.0	5.27	46.4
2	no turb.	1024	50	25	35.0	11.7	18.7	16.4	2245	12.8	15.9	37.8	4.98	42.7
3	no turb.	1024	50	25	50.0	19.6	31.9	16.0	2370	15.0	3.7	5.2	3.40	24.1
4	no turb.	1024	50	25	50.0	18.9	32.4	15.2	2375	14.9	4.1	5.9	3.42	23.2
5	no turb.	1024	50	25	50.0	21.3	34.9	15.6	2375	14.8	3.8	5.8	3.38	24.2
6	no turb.	1024	50	25	70.0	34.4	45.7	15.2	2388	15.4	1.1	1.4	2.98	18.7
7	no turb.	1024	50	25	70.0	28.5	43.7	15.4	2385	15.3	1.3	2.2	3.44	25.5
8	no turb.	1024	50	25	70.0	29.2	37.6	15.5	2385	15.6	1.4	2.1	3.49	23.3
9	no turb.	1024	50	25	105.0	46.0	50.5	15.2	2392	15.6	0.2	0.3	2.85	20.2
10	Onishi	1024	50	25	35.0	8.4	20.2	13.9	2213	10.7	18.0	41.8	5.11	43.5
11	Onishi	1024	50	25	35.0	6.2	17.7	14.4	2180	10.4	15.8	43.9	5.83	51.7
12	Onishi	1024	50	25	50.0	16.8	29.0	16.7	2351	15.0	9.4	17.0	4.45	32.4
13	Onishi	1024	50	25	50.0	13.0	25.7	18.1	2317	14.6	12.5	29.3	5.64	37.5
14	Onishi	1024	50	25	50.0	13.6	27.2	16.9	2337	15.4	13.4	30.1	5.34	40.8
15	Onishi	1024	50	25	50.0	12.8	25.1	19.4	2308	15.9	14.0	33.1	5.85	44.1
16	Onishi	1024	50	25	50.0	14.2	24.9	17.8	2295	15.0	16.3	42.5	6.31	46.8
16*	Onishi, au-only	1024	50	25	50.0	16.8	28.8	16.3	2362	15.0	8.7	15.2	3.89	31.6
17	Onishi	1024	50	25	70.0	19.2	36.4	15.2	2370	14.8	3.0	4.6	4.00	24.9
18	Onishi	1024	50	25	70.0	21.7	38.2	15.3	2377	15.1	2.8	4.4	3.86	24.4
19	Onishi	1024	50	25	70.0	21.4	36.7	15.5	2377	15.2	2.9	4.4	3.88	25.4
20	Onishi	1024	50	25	70.0	24.0	33.5	15.8	2378	15.4	3.2	5.0	4.01	25.5
21	Onishi	1024	50	25	105.0	30.7	43.1	15.3	2392	15.5	0.9	1.6	4.37	27.7
22	Ayala-Wang	1024	50	25	35.0	4.8	13.6	10.5	2016	6.4	11.5	34.2	5.47	53.5
23	Ayala-Wang	1024	50	25	35.0	4.4	13.7	12.7	1901	7.6	14.1	46.2	6.68	62.6
24	Ayala-Wang	1024	50	25	50.0	5.6	17.8	13.6	2123	9.9	14.3	41.2	6.18	51.6
25	Ayala-Wang	1024	50	25	50.0	6.4	15.8	14.1	2091	9.7	15.2	48.3	7.82	61.3
26	Ayala-Wang	1024	50	25	50.0	6.1	18.0	15.0	2143	10.5	15.8	47.5	6.55	55.6
27	Ayala-Wang	1024	50	25	50.0	7.2	18.2	14.0	2151	10.4	15.3	41.8	5.82	48.3
28	Ayala-Wang	1024	50	25	70.0	13.7	26.2	16.4	2309	14.0	12.7	30.2	5.54	41.8
29	Ayala-Wang	1024	50	25	70.0	9.7	22.0	17.8	2265	13.5	15.3	42.7	6.63	49.6
30	Ayala-Wang	1024	50	25	70.0	10.6	21.4	17.5	2244	13.2	14.6	42.0	6.65	50.3
31	Ayala-Wang	1024	50	25	105.0	19.3	35.2	15.9	2364	15.1	4.7	9.5	4.95	33.9

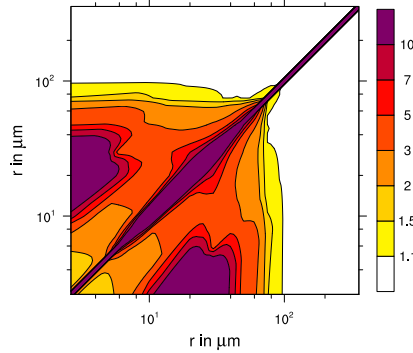
Table 3. As previous Table, but for the simulations to investigate the resolution dependency at $N_c = 50 \text{ cm}^{-3}$.

n	kernel	N_x	Δx	Δz	N_c	t_1	t_2	C	z_i	CWP	RWP	R	AC/AU	RE
1	no turb.	2048	25	25	50.0	7.4	15.4	13.2	2072	10.4	10.7	33.1	8.00	56.4
2	no turb.	2048	25	25	50.0	7.9	20.4	17.1	2195	14.0	13.5	38.2	6.72	51.0
3	no turb.	2048	25	25	50.0	7.7	16.3	15.0	2052	10.8	14.3	47.0	9.01	61.6
4	no turb.	1024	50	25	50.0	19.6	31.9	16.0	2370	15.0	3.7	5.2	3.40	24.1
5	no turb.	1024	50	25	50.0	18.9	32.4	15.2	2375	14.9	4.1	5.9	3.42	23.2
6	no turb.	1024	50	25	50.0	21.3	34.9	15.6	2375	14.8	3.8	5.8	3.38	24.2
7	no turb.	512	100	25	50.0	24.1	46.7	12.4	2422	12.8	2.8	3.4	2.88	16.1
8	Onishi	2048	25	25	50.0	7.3	17.3	14.4	2066	11.1	13.8	44.8	8.05	59.5
9	Onishi	2048	25	25	50.0	6.2	16.0	14.6	2062	10.3	12.9	42.0	8.92	61.4
10	Onishi	1024	50	25	50.0	16.8	29.0	16.7	2351	15.0	9.4	17.0	4.45	32.4
11	Onishi	1024	50	25	50.0	13.0	25.7	18.1	2317	14.6	12.5	29.3	5.64	37.5
12	Onishi	1024	50	25	50.0	13.6	27.2	16.9	2337	15.4	13.4	30.1	5.34	40.8
13	Onishi	1024	50	25	50.0	12.8	25.1	19.4	2308	15.9	14.0	33.1	5.85	44.1
14	Onishi	1024	50	25	50.0	14.2	24.9	17.8	2295	15.0	16.3	42.5	6.31	46.8
15	Onishi	512	100	25	50.0	16.0	33.7	13.0	2398	12.5	7.4	12.3	3.96	26.8
16	Ayala-Wang	2048	25	25	50.0	4.7	12.7	10.6	1939	7.3	10.2	34.7	7.79	59.1
17	Ayala-Wang	1024	50	25	50.0	5.6	17.8	13.6	2123	9.9	14.3	41.2	6.18	51.6
18	Ayala-Wang	1024	50	25	50.0	6.4	15.8	14.1	2091	9.7	15.2	48.3	7.82	61.3
19	Ayala-Wang	1024	50	25	50.0	6.1	18.0	15.0	2143	10.5	15.8	47.5	6.55	55.6
20	Ayala-Wang	1024	50	25	50.0	7.2	18.2	14.0	2151	10.4	15.3	41.8	5.82	48.3
21	Ayala-Wang	512	100	25	50.0	6.1	22.9	11.4	2321	9.5	14.5	31.2	4.48	36.8

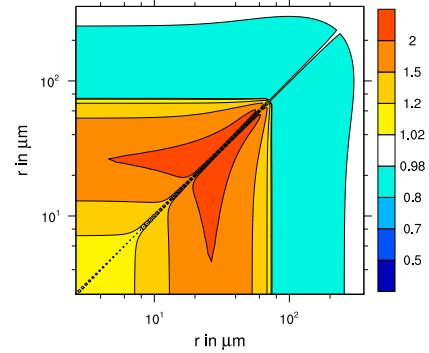
a) Ayala-Wang kernel, $Re_\lambda = 1000$



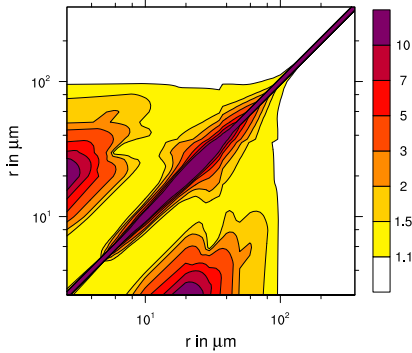
b) Ayala-Wang kernel, $Re_\lambda = 20000$



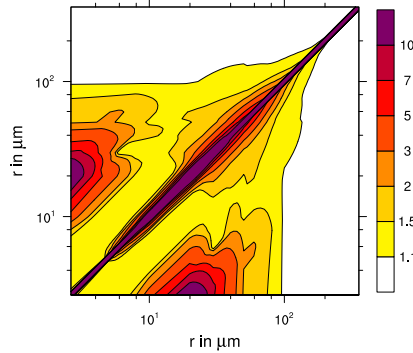
c) Ayala-Wang kernel, difference



d) Onishi kernel, $Re_\lambda = 1000$



e) Onishi kernel, $Re_\lambda = 20000$



f) Onishi kernel, difference

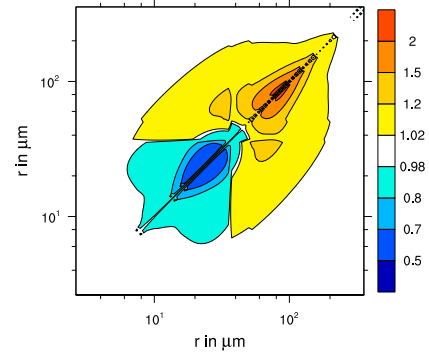


Figure 1. Enhancement factor of the collision-coalescence kernel for a dissipation rate of $\epsilon = 1000 \text{ cm}^2\text{s}^{-3}$. Shown are (a) the Ayala-Wang kernel for a Taylor-microscale Reynolds number of 1000, (b) the Ayala-Wang kernel for $Re_\lambda = 20000$, (c) the ratio of the Ayala-Wang kernel at $Re_\lambda = 20000$ and $Re_\lambda = 1000$. The second row show the same plot for the Onishi kernel at $\epsilon = 1000 \text{ cm}^2\text{s}^{-3}$ and (d) $Re_\lambda = 1000$, (e) $Re_\lambda = 20000$ and (f) the ratio between the kernels at those two Reynolds numbers.

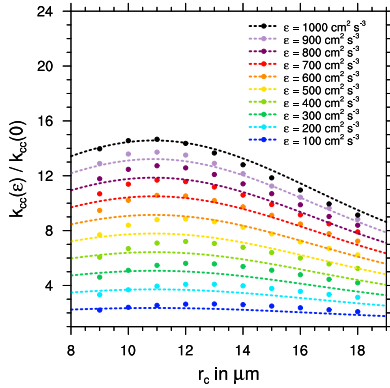
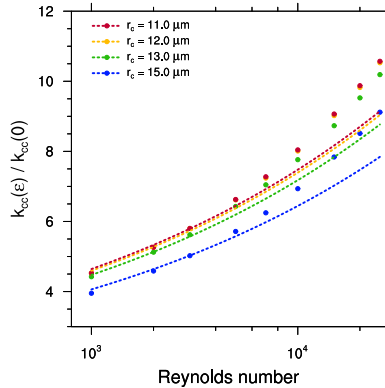
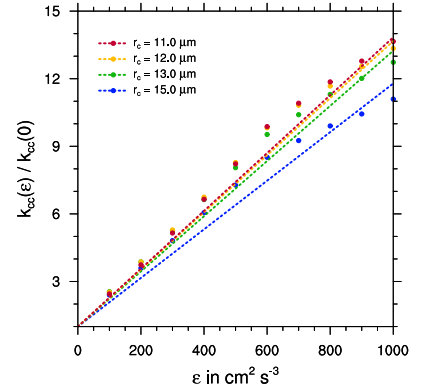
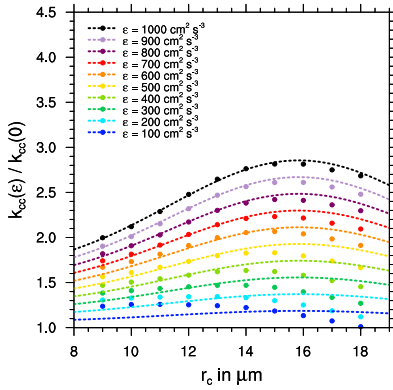
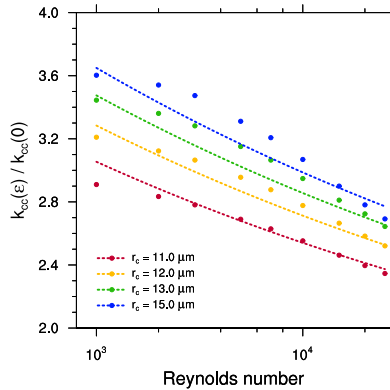
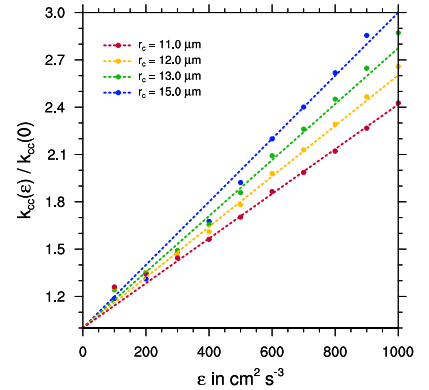
a) Ayala-Wang kernel, $Re_\lambda = 20000$ b) Ayala-Wang kernel, Re_λ -dependencyc) Ayala-Wang kernel, ϵ -dependencyd) Onishi kernel, $Re_\lambda = 20000$ e) Onishi kernel, Re_λ -dependencyf) Onishi kernel, ϵ -dependency

Figure 2. Enhancement factor of the autoconversion rate for the Ayala-Wang kernel (upper row) and the Onishi kernel (lower row) at $Re_\lambda = 20000$ (a,c), the Reynolds number dependency of the enhancement factor at $\epsilon = 600 \text{ cm}^2 \text{ s}^{-3}$ (b,d), and the dependency on dissipation rate for $Re_\lambda = 20000$ (c,f). Data points (dots) are based on numerical solutions of the stochastic collection equation (SCE), the parameterization shown (dashed lines) is Eq. (10) with the coefficients as given in Table 1. All plots are shown for $\nu = 1$. Note the different scaling of the y-axis for both kernels.

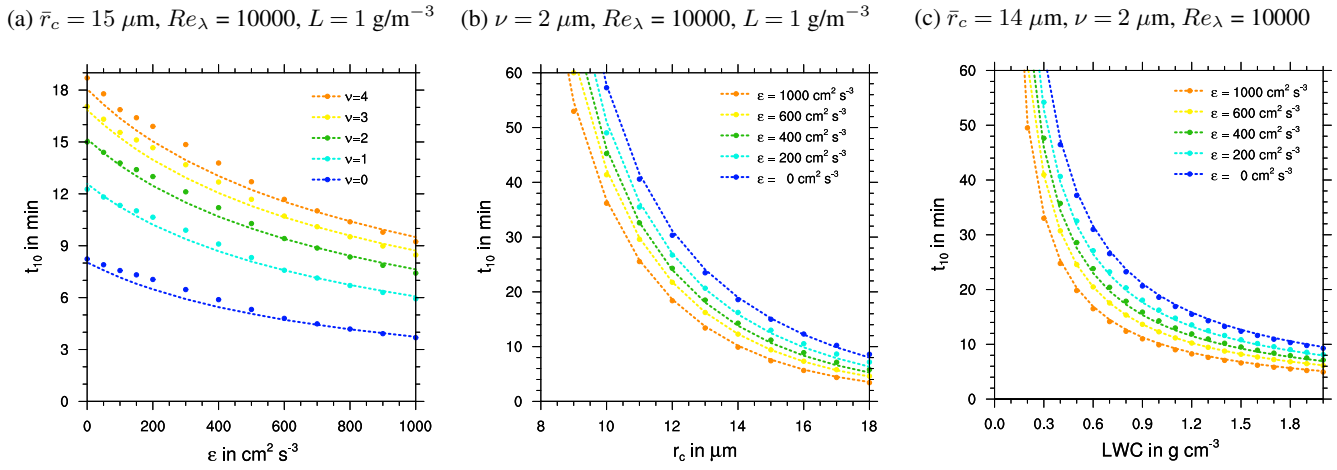


Figure 3. Time t_{10} , that is needed to convert 10 % of the initial cloud water to rain water (a) t_{10} as a function of dissipation rate ϵ for various ν (and $\bar{r}_c = 15 \mu\text{m}$, $Re_\lambda = 10000$), (b) t_{10} as a function of mean cloud droplet radius \bar{r}_c for various values of dissipation rate ϵ (and $\nu = 2$, $Re_\lambda = 10000$) and (c) t_{10} as a function of the initial cloud liquid water content for various values of dissipation rate ϵ (and $\bar{r}_c = 14$, $\nu = 2$, $Re_\lambda = 10000$). Data points are numerical solution of the SCE, dashed lines represent the solutions of the two-moment bulk scheme with the enhancement factor for autoconversion based on the Onishi kernel as given by Eq. (10) and the coefficients of Table 1.

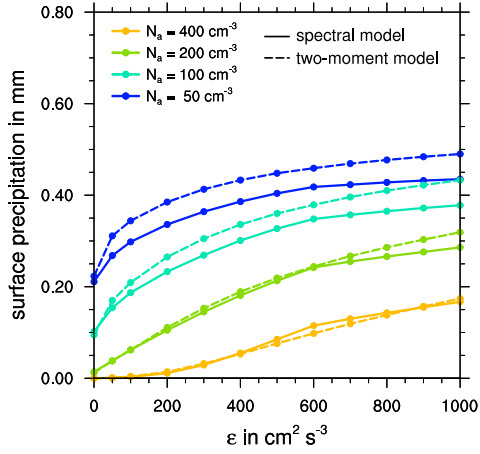
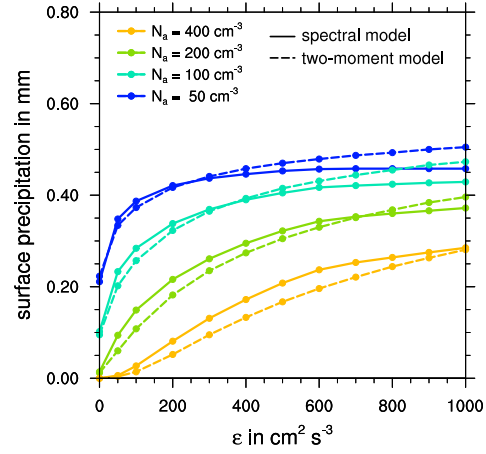
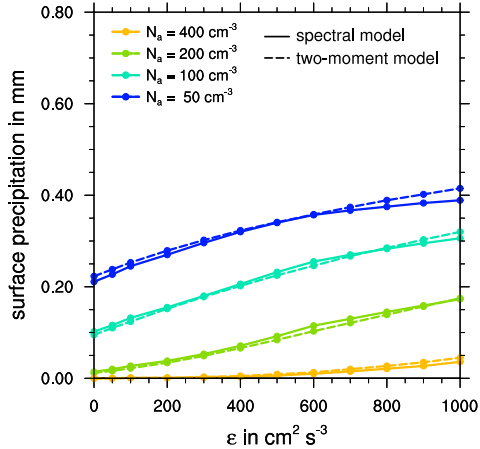
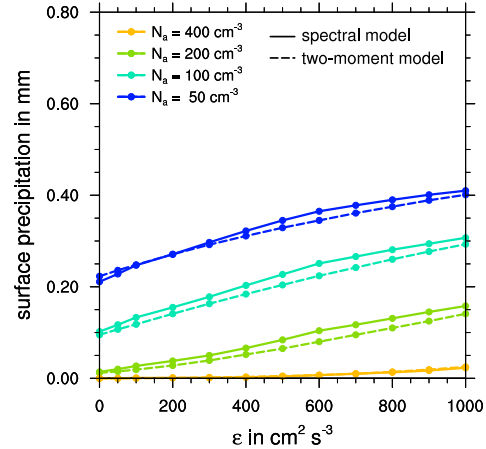
(a) Ayala-Wang kernel, $Re_\lambda = 1000$ (b) Ayala-Wang kernel, $Re_\lambda = 20000$ (c) Onishi kernel, $Re_\lambda = 1000$ (d) Onishi kernel, $Re_\lambda = 20000$ 

Figure 4. Accumulated surface precipitation of the 1D kinematic model as a function of the assumed in-cloud turbulent dissipation rate ϵ (other parameters are temperature gradient $\Gamma_0 = 1.5$ K/km, the maximum updraft speed $w_0 = 2$ m/s, and the updraft time scale $\tau_w = 40$ min). Shown are results from the Ayala-Wang model at $Re_\lambda = 1000$ (a) and $Re_\lambda = 20000$ (b), as well as the Onishi model at those two Reynolds numbers (c,d). Results of the spectral bin reference model are depicted with solid lines, the results of the two-moment parameterization with dashed lines.

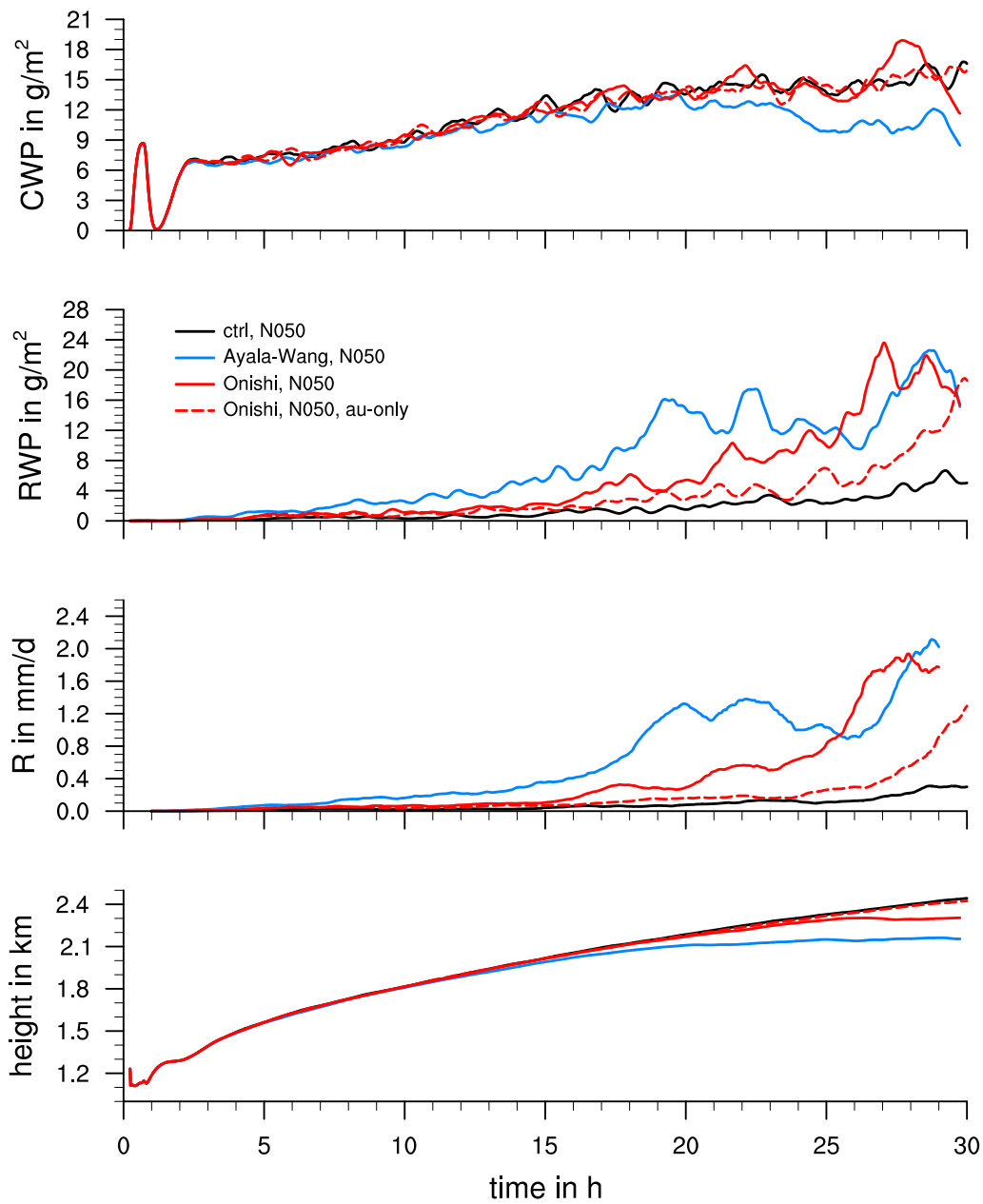
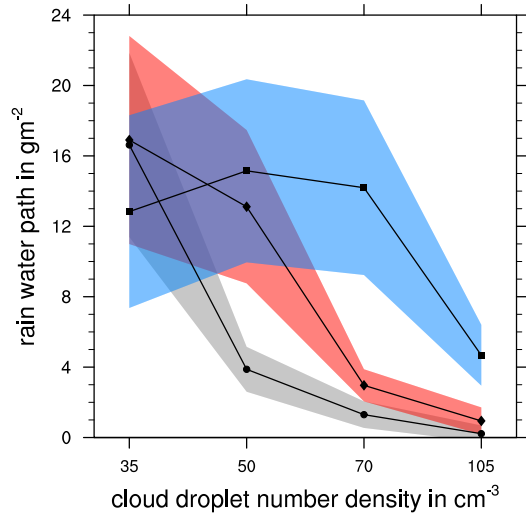
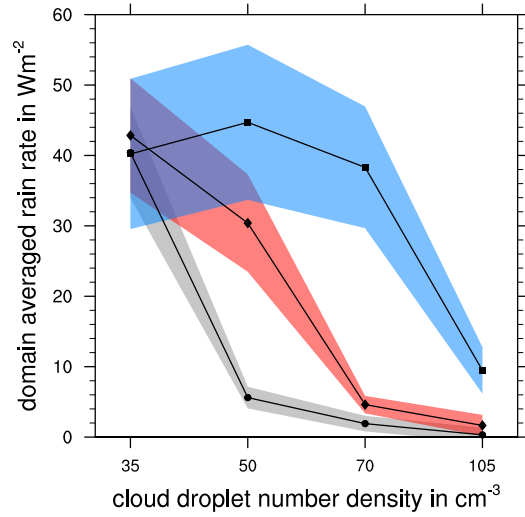


Figure 5. Time series of the cloud liquid water path, rain water path, the surface rain rate and the inversion height for four simulations using the three different collection kernels. The simulation marked 'au-only' applies the turbulent enhancement only to autoconversion, but ignores the effect on accretion. We have applied a running average to all time series with an averaging window of 120 min for the surface rain rate and 30 min for RWP, CWP and inversion height.

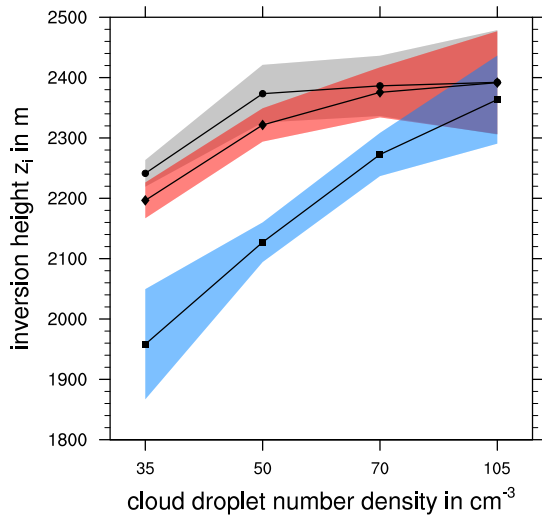
(a) rain water path



(b) surface rain rate



(c) inversion height



(d) accretion-autoconversion ratio

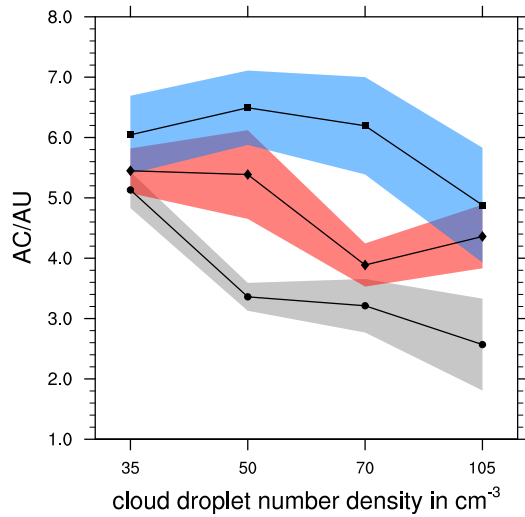


Figure 6. Sensitivity of LES results to variations in the cloud droplet number density. Shown are the rain water path, surface rain rate, inversion height, and the accretion-autoconversion ratio for the three different collection kernels of the control simulations using the purely gravitational kernel (bullets, grey shading), the Ayala-Wang kernel (squares, blue shading), and the Onishi kernel (diamonds, red shading). The shaded area indicates the standard error at a 95 % confidence level.

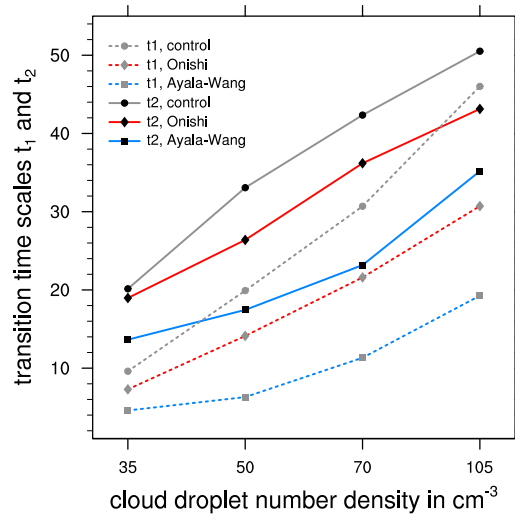
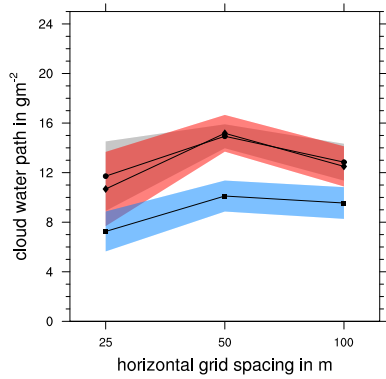
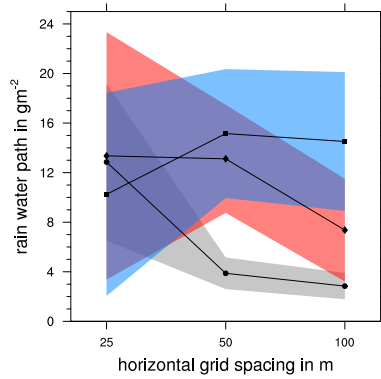


Figure 7. Transition time scales t_1 (dashed, grey symbols) and t_2 (solid, black symbols) defined as the time when the domain-averaged rain rate exceeds 0.1 mm/d or 0.8 mm/d, respectively, for the first time. The transition times are averaged over multiple simulations with different random seeds.

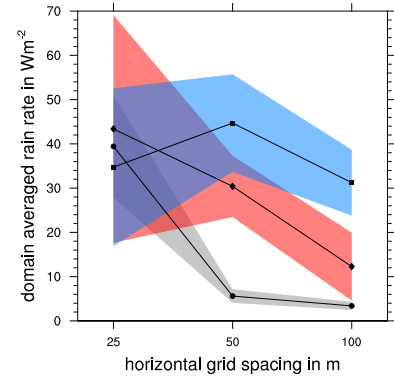
(a) cloud water path



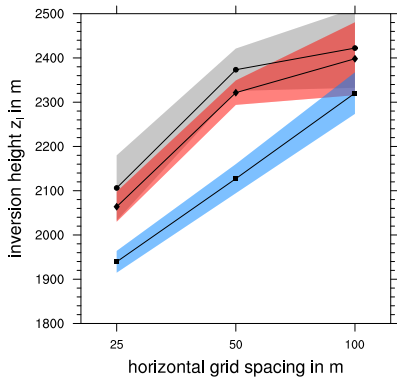
(b) rain water path



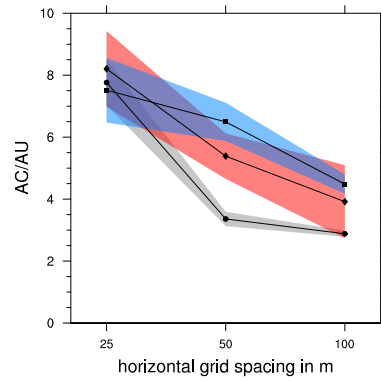
(c) surface rain rate



(c) inversion height



(d) accretion-autoconversion ratio



(d) rain efficiency

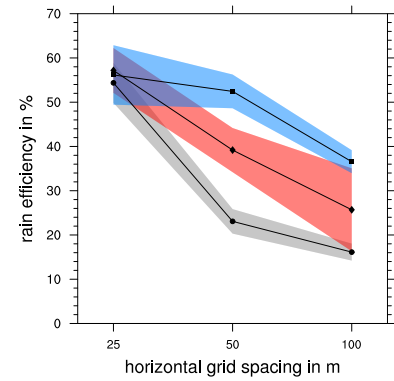


Figure 8. As Fig. 6, but showing the dependency of the results in the sampling period 24 h to 30 h on grid spacing for a cloud droplet number density of $N_c = 50 \text{ cm}^{-3}$.

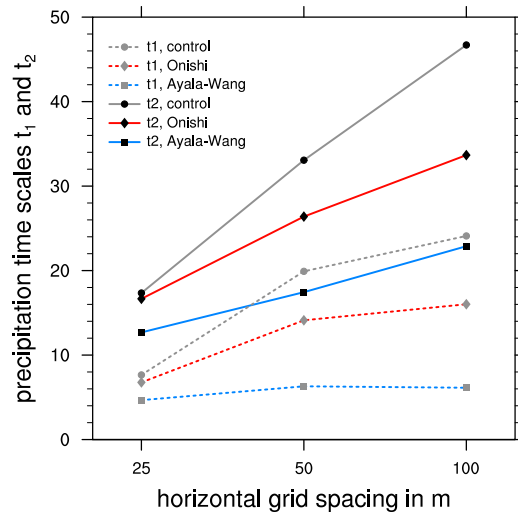


Figure 9. As Figure 7, but showing the dependency of the rain formation time scales t_1 and t_2 on horizontal grid spacing for a cloud droplet number density of 50 cm^{-3} .